UNCERTAINTY IN EMISSIONS PATHWAYS AND EARTH SYSTEM DYNAMICS: IMPLICATIONS FOR GLOBAL MEAN SEA LEVEL RISE

A Thesis

Presented to the Faculty of the Graduate School

of Cornell University

in Partial Fulfillment of the Requirements for the Degree of

Master of Science

by

Chloe Darnell

August 2023

ABSTRACT

Global mean sea level rise (GMSLR) poses many climate risks, such as coastal flooding and erosion. Managing the risks associated with GMSLR can involve a balance between mitigation and adaptation, but the near-term effectiveness of CO_2 emissions reductions is limited since GMSLR responds to emissions on centennial to millennial timescales. An improved understanding of relevant human-Earth interactions can provide insight into the risks associated with GMSLR and how they evolve over time. Previous studies on the interactions between uncertain emissions pathways and uncertainties in the Earth system response that result in GMSLR have been restricted to a small number of pre-defined scenarios. Here, we use a large ensemble of CO_2 emissions trajectories to force a calibrated Earth system model, which simulates warming and sea level rise. Using this framework, we generate projections for radiative forcing, temperature, and GMSLR under different emissions pathways, as well as relative contributions from each component of GMSLR. We then conduct a global sensitivity analysis over uncertain emissions pathways, the carbon cycle, and climate and ice sheet dynamics. To analyze how different decarbonization strategies alter GMSLR outcomes and uncertainties, we categorize the results into different groups by emissions peaking time, which serve as a proxy for the level of mitigation ambition. From the sensitivity analysis, we find that uncertainties in emissions drive the most variance in GMSLR in the medium-to-long-term. Prior to 2070, Earth system dynamics, particularly those related to the Antarctic Ice Sheet, have the most influence on GMSLR, but between 2070 and 2100, a transition occurs as variability in emissions begins to heavily control GMSLR outcomes. We also find that GMSLR outcomes are likely to be sufficiently high to necessitate adaption

regardless of when CO_2 emissions peak, and even rapid mitigation cannot fully manage the risks posed by sea level rise. For the relative contributions from each component of GMSLR, there are differences depending on peaking group and timescale. Under lower-emissions pathways in the near-term, thermal expansion plays a larger role in GMSLR, but in the longer-term, the Antarctic Ice Sheet and Greenland Ice Sheet contributions dominate. Under higher-emissions pathways, the ice sheets dominate in all time periods. Both the Antarctic and Greenland Ice Sheets are also subject to the most uncertainty in future projections. Due to the large potential of the ice sheets to contribute substantially to GMSLR outcomes, characterizing the uncertainties associated with their melting is crucial to better understand future climate risks. The representation of ice sheet melting dynamics plays an important role in projecting GMSLR, and this analysis highlights the need for future studies to consider whether the simplistic melting dynamics modeled for the Greenland Ice Sheet are a suitable approximation of real-world outcomes.

BIOGRAPHICAL SKETCH

Chloe Darnell grew up in Crown Point, Indiana, where she graduated from high school in 2017. She then earned a Bachelor of Science in Civil Engineering at the University of Kentucky in 2021, with minors in Spanish and Mathematics. During her undergraduate education, Chloe conducted research involving life cycle assessment and the energy-water nexus. After graduating, she began a Master of Science at Cornell University in the fall of 2021, where she joined the Srikrishnan Research Group in the Department of Biological and Environmental Engineering. During her graduate studies, Chloe worked at the National Renewable Energy Laboratory, where she researched the feasibility of freshwater alternatives for a variety of end-use scenarios. Broadly, Chloe hopes to use the skills she has developed throughout her education to better understand the human-Earth system and guide sustainable decision-making.

ACKNOWLEDGEMENTS

The process of research is inevitably filled with obstacles and unforeseen issues, and I am so grateful to have a wonderful network of people whose support has helped me persevere despite these challenges. First, I would like to thank my advisor, Dr. Vivek Srikrishnan, for the immense amount of time and dedication that you have invested in my success. It is an honor to be your first graduating student at Cornell, and it has been inspiring to look back and see how much my knowledge and research abilities have developed under your guidance as a mentor. I also want to express my appreciation to my committee member, Dr. Flavio Lehner, whose kind words and feedback helped me bring my thesis to its full potential. To Lisa Rennels, Frank Errickson, and Tony Wong, thank you for your work in developing the tools that made this thesis possible, and for your help with questions that came up along the way.

I am also very grateful for my lab mates: Parin Bhaduri and Katerina Tang. It has been an absolute pleasure becoming friends and getting to know both of you throughout my time here, and our shared laughs and conversations helped me through many difficulties over the past two years. You are both such hard-working, kind-hearted people, and I am so excited to see the amazing things that you both do throughout the rest of your degrees and beyond. Thank you also to my friend, Rohini Gupta. I am so grateful for your willingness to help me whenever I needed it, and I truly admire your drive and passion for the work that you do. Your kind, friendly personality made me feel welcome from the first day that we met, and the effort that you put in to organize events and include others is an integral part in making the EWRS group into a community.

To my undergrad advisor, Dr. Diana Byrne, I want to let you know how much I appreciate you fostering my interest in research. Your kindness and encouragement inspired me to be the best version of myself, and I sincerely appreciate your guidance throughout the grad school application process that brought me here.

I would also like to express my appreciation for my family, whose love and support throughout my life taught me to believe in myself and my potential. Specifically, thank you to my mother, who would always lend an ear about my day during our phone calls down the hill. Whether I was talking about exciting news or a hardship I was facing, you always listened and offered endless support and encouragement. Finally, to my partner Diego, I truly could not have done this without you. From making me food during a long work session to listening to me talk about the intricacies of my research, you have supported me and stood by my side every single step of the way. You brighten my life even at my lowest points, and I am extremely lucky that you moved here with me. As our time here comes to a close, I am so excited to see what the next chapter of our lives brings.

TABLE OF CONTENTS

LIST OF FIGURES

LIST OF TABLES

1. INTRODUCTION

1.1. Uncertainty and Climate Risks

As a result of anthropogenic climate change, global mean sea level is increasing, which leads to climate risks such as coastal flooding and erosion (Church et al., 2008). Extreme sea levels and flooding events are estimated to increase in frequency in many coastal areas around the world, even under low emissions scenarios that limit warming to 1.5°C (Tebaldi et al., 2021). Managing risks is difficult since the coupled human-Earth system is highly complex, consisting of feedbacks, tipping points, and interacting processes. Earth system processes may also be altered as the climate warms, such as a decreased proportion of land and ocean uptake of CO_2 emissions (IPCC, 2021). Managing these risks is further complicated by the inertia of the climate system, which creates a lag in the Earth system response to reductions in emissions (Hansen et al., 1985). Even after anthropogenic greenhouse gas (GHG) emissions cease, global mean sea level will continue to rise on centennial to millennial timescales as a result of deep-ocean warming and ice-sheet melt (IPCC, 2021). Global mean sea levels are likely to be even more affected by climate inertia and committed warming than global mean temperature (Meehl et al., 2005, 2012). Even if GHG concentrations were stabilized today, it would take about one hundred years for temperature to level off, but sea level rise from thermal expansion would continue to increase for centuries, even without taking melting from ice sheets and glaciers into account (Meehl et al., 2005). Since global mean sea level rise (GMSLR) will continue on long timescales after emissions are stabilized, mitigation is likely insufficient to

manage the risk it poses, and adaptation measures must also be adopted to manage sea level impacts (Meehl et al., 2012).

Due to these complex system dynamics, GMSLR risks can cascade and compound over time. Socioeconomic factors influence emissions trajectories, which then alter the Earth system and lead to climate impacts. These climate impacts then influence the human system, leading to a feedback loop (Figure 1) (Keller et al., 2021). To manage the risks associated with this climate change feedback loop, different types of decision levers can be implemented. There are four main categories of relevant decision levers: mitigation, carbon sequestration, solar radiation management, and adaptation. Mitigation consists of reducing GHG emissions, whereas carbon sequestration involves removing and storing CO_2 from the atmosphere after emissions have been produced. Solar radiation management aims to alter the Earth system response to GHGs in the atmosphere, which includes strategies such as cloud seeding or aerosol injections (Keller et al., 2021). The final lever, adaptation, involves adjusting to the effects of climate change.

Here, we focus on the mitigation and adaptation levers and explore the interactions between them. Mitigation and adaptation operate on different spatiotemporal scales, which results in different objectives and approaches for each lever. Mitigation affects the global climate system on medium-to-long-term timescales, whereas adaptation operates locally on a short-term timescale. The effectiveness of both mitigation and adaptation are also subject to many key uncertainties, such as climate sensitivity (the projected equilibrium temperature change for a doubling of carbon dioxide concentration) and uncertainty in climate

carbon-cycle feedbacks when emissions are converted to atmospheric concentrations (Lamontagne et al., 2019; Lee et al., 2021). When progressing through the climate feedback loop, these uncertainties compound as additional uncertain system processes are included to produce the next outcome.

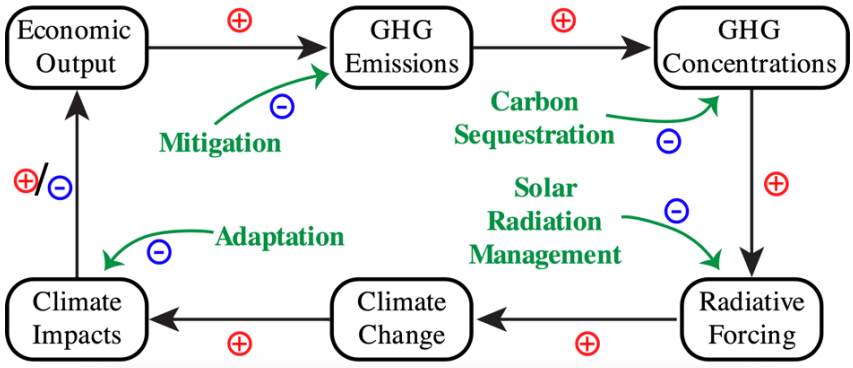

Figure 1. Climate change feedback loop. Adapted from Keller et al. (2021).

As the uncertainties compound in the feedback loop, the total uncertainty in future climate projections increases. Many human and Earth system processes are also subject to "deep" uncertainty, which is the condition where experts do not know or have not reached a consensus about system boundaries, outcomes of interest and their importance, or the prior probabilities of parameters in a system model (Lempert & Collins, 2007; Reed et al., 2023). In the human system, for example, it is deeply uncertain which emissions pathways will be followed in the future (Wong & Keller, 2017). In the Earth system, an example of a deeply uncertain process is the threshold behavior of the Antarctic Ice Sheet, which could potentially lead to rapid disintegration of large parts of the ice sheet (Alley et al., 2015; Pattyn et al., 2018; Pollard et al., 2015; Wong & Keller, 2017). The West Antarctic Ice Sheet (WAIS) is

particularly susceptible to such behavior since a large portion of it is a marine ice sheet (i.e., it sits on bedrock below sea level) (Pollard et al., 2015). The grounded parts of the WAIS are attached to ice shelves (the floating portion of the ice sheet that extends into the ocean), and the ice shelves are in direct contact with the ocean and thus vulnerable to melting from the ocean as it warms. Another factor that makes the WAIS particularly vulnerable to melting is the slope of its grounding line, or the region where the grounded ice sheet transitions to an ice shelf. Many parts of the WAIS have a grounding line on a retrograde bed slope that deepens toward the center of the ice sheet (Pattyn et al., 2018). As the underside of the ice shelves melt due to the direct contact with the ocean, the grounding line retreats, which leads to additional ice flux and runaway retreat due to the retrograde slope. This positive feedback is referred to as Marine Ice Sheet Instability (MISI), and it may cause large parts of the WAIS to rapidly disintegrate (Alley et al., 2015; Pattyn et al., 2018; Pollard et al., 2015). The ocean warming can also create crevasses and fractures in ice shelves, which weakens their ability to support the interior ice. This behavior, called hydrofracturing, can cause ice shelves to rapidly disintegrate to produce steep, unstable ice cliffs. These shear ice cliffs are then susceptible to collapse from their own weight in a process called Marine Ice Cliff Instability (MICI) (Pattyn et al., 2018; Ruckert et al., 2017). Due to the deep uncertainty surrounding both MISI and MICI, a consensus has not been reached about whether these processes will occur, and if they do occur, how much they will contribute to global sea level (Wong & Keller, 2017).

To explore the implications of deeply uncertain outcomes such as future emissions and rapid melting dynamics, projections from models are a useful tool for

characterizing uncertainties and examining potential drivers of outcomes of interest. Since it is not possible to verify a model and prove it to be a true representation of a system (Oreskes et al., 1994), models can instead be used to explore uncertainty using statistical analyses across a variety of states-of-the-world (SOWs). Complex models, such as those representing Earth system processes, may more accurately represent real-world conditions, but are more computationally expensive than simpler models. Uncertainty characterization and quantification require running a model many times with different inputs, which can be computationally infeasible for complex models with long run times (Helgeson et al., 2021). This creates a tradeoff between model complexity and computational expense, called the performance-complexity tradeoff (Reed et al., 2023). As a result, simpler models can more effectively characterize the uncertainty associated with Earth system processes that drive climate risks.

1.2. Contributors to Global Mean Sea Level Rise

Due to the climate risks that GMSLR poses, it is important to understand the mechanisms that contribute to sea level changes, which allows for improved uncertainty characterization in GMSLR projections. Global mean sea level changes are a result of two mechanisms: density changes and mass changes (Fox-Kemper et al., 2021). The mass changes in the ocean are a result of melting of the terrestrial cryosphere and changes in land-water storage, while the density changes result from variations in the temperature and salinity of the ocean (Milne et al., 2009). Although the contribution from salinity-based density changes can lead to regional sea level variations, they do not contribute to global mean sea level since the total salt content

of the ocean remains essentially constant (Cazenave & Llovel, 2010). Here, we focus on global mean sea level changes, so salinity-based density changes and the resulting regional sea level variations and are not in the scope of this paper. Instead, we consider temperature-based changes since they primarily drive the density-driven changes in the global mean sea level. As the ocean temperature increases, its additional heat content causes the ocean waters to expand, which is referred to as thermal expansion. Therefore, the main contributors to GMSLR from mass changes are the Antarctic Ice Sheet, the Greenland Ice Sheet, glaciers and small ice caps, and land-water storage, and the main contributor to GMSLR from density changes is thermal expansion.

1.2.1. Thermal Expansion

Thermal expansion has a large impact on global sea level, accounting for the largest contribution to GMSLR on average over the 20th century (WCRP Global Sea Level Budget Group, 2018). This is because the ocean has taken up about 93% of the excess heat associated with anthropogenic emissions from 1971 to 2010, leading to an increase in ocean temperature (Johnson & Lyman, 2020; WCRP Global Sea Level Budget Group, 2018). As the oceans warm, the density of the water decreases and the volume per unit of mass increases (Fox-Kemper et al., 2021). The excess energy taken up by the oceans leads to an increase in ocean heat content, which has created increasingly dominant warming trends in ocean heat content globally (Johnson & Lyman, 2020). Hough & Wong (2022) projects that the short-term risks associated with GMSLR are mainly driven by thermal expansion, but the long-term risks are driven by ice sheet loss from the Antarctic and Greenland Ice Sheets.

1.2.2. Ice Sheets

There are two ice sheets in the world: the Antarctic Ice Sheet (AIS) and the Greenland Ice Sheet (GIS), which are the largest reservoirs of frozen freshwater on the planet (Fox-Kemper et al., 2021). The melting of the two ice sheets has increased substantially in recent years, resulting in a larger sea level contribution. Combined, the AIS and the GIS have lost mass at an average rate of 372 gigatonnes per year from 2016 to 2020, which is much greater than their 1992-1996 mass loss rate of 105 gigatonnes per year (Otosaka et al., 2023). This increase in melting rate is the result of a warming climate combined with a variety of other factors, including potential thresholds and instability. As discussed previously, melting in the WAIS is susceptible to the deeply uncertain processes of MISI and MICI, which may be triggered past a certain threshold. These processes can result in rapid melting of large portions of the WAIS and therefore contribute substantially to GMSLR. However, the WAIS is not the only region vulnerable to such threshold behavior. Both the AIS and the GIS are susceptible to tipping points, which refer to "critical thresholds in a system that, when exceeded, can lead to a significant change in the state of the system, often with an understanding that the change is irreversible" (Hoegh-Guldberg et al., 2018). Although the two ice sheets both have tipping points, they have different defining characteristics that impact their contribution to GMSLR, so we discuss them separately.

The AIS is composed of two distinct regions: the WAIS and the East Antarctic Ice Sheet (EAIS). The EAIS contains a much larger volume of ice than the WAIS, amounting to 52.2 meters of sea-level equivalent (SLE) compared to the 5.3 meters SLE in the WAIS (Pattyn & Morlighem, 2020). Contrary to the WAIS, which is a

marine ice sheet, most of the EAIS lies on land well above sea level where it is not in direct contact with the ocean, making it less vulnerable to warming than the WAIS. Even so, the marine parts of the EAIS may be susceptible to similar processes causing instability like those in the WAIS, including MISI and grounding-line retreat (Stokes et al., 2022). However, there is currently insufficient evidence to determine if the marine parts of the EAIS will reach thresholds triggering instability (Stokes et al., 2022). Due to this lack of evidence, the EAIS is the most uncertain component of the AIS mass balance (Otosaka et al., 2023).

The other region of the AIS, the WAIS, has been the subject of much debate regarding its stability and role in future GMSLR. Previous literature showcases a wide range of beliefs on the stability of the WAIS over the years, ranging in beliefs that the ice sheet is stable, unstable, or naturally oscillatory (Oppenheimer et al., 2008). Today, the future of the WAIS is still under debate. Joughin et al. (2014) suggests that MISI and the subsequent collapse of the Thwaites Glacier, a vast glacier that drains about 10% of the WAIS, is potentially underway, but rapid collapse of the glacier may not occur for another 200 to 900 years. Another study finds that Pine Island Glacier in the WAIS quadrupled its thinning rate from 1992 to 2008 as a result of MISI, so mass losses are likely to continue and move further inland (Rignot et al., 2011). Conversely, Urruty et al. (2022) argues that in the present day, the grounding-line retreat of the marine portions of the AIS is driven solely by external climate forcing, and irreversible retreat from MISI has not been triggered. Reese et al. (2022) proposes that although MISI has not been triggered in the present, the grounding lines of the Thwaites Glacier may transition toward MISI and a subsequent collapse if current

climate conditions persist in the future. Specifically, Wong, Bakker, and Keller (2017) estimates that a global temperature increase of 1.9 to 3.1°C will trigger a rapid disintegration of the AIS.

Although the stability the AIS is still under debate, a variety of studies have emerged that shed light on specific factors that impact its vulnerability to unstable dynamics. The bed topography varies across the AIS, so different areas are more prone to MISI and other melting processes than others, with features such as a retrograde slope or nearby deep glacial trough leading to increased vulnerabilities (Morlighem et al., 2020). The additional process of MICI may make an area more susceptible to MISI, and neglecting MICI in models may lead to a low-bias for sea level projections (Ruckert et al., 2017). Bassis et al. (2021) suggests that MICI does not always lead to catastrophic collapse of a glacier though, and it is strongly dependent on glacial geometry. The study finds that a key factor is the ice thickness gradient, which is how quickly the ice thickness increases upstream from an ice cliff. If the ice thickness gradient passes a critical threshold, the glacier is susceptible to runaway collapse, but it can still be stabilized via resistive forces such as icebergs or sea ice (Bassis et al., 2021). Outside of MISI and MICI, other factors also play an important role in the melting rate of the AIS. Artemieva (2022) finds that the rate of melting at the underside of the ice sheet (basal melting) in the Antarctic has been substantially underestimated due to processes in the deep Earth, such as high mantle heat and the thickness of the lithosphere. This leads to a higher heat flux than previously estimated, which may promote additional sliding and a significant reduction in ice mass. Another study concludes that the eastern ice shelf of Thwaites Glacier has a grounding line that

is considerably warmer than previously thought, which implies that basal melting has been strongly suppressed (Davis et al., 2023). As a result, even moderate basal melting rates may cause grounding-line retreat to occur rapidly with potential instability (Davis et al., 2023).

Like the AIS, there is also much debate surrounding the melting rate and stability of the GIS. The GIS has already undergone considerable melting, and from 1994 to 2013 it experienced a 250% to 575% increase in melt intensity relative to pre-industrial values (Trusel et al., 2018). Contrary to the AIS, the GIS is a terrestrial ice sheet and mostly experiences melting from above due to the lack of direct contact with the ocean. This leads to several positive feedback mechanisms: the melt-elevation feedback and the melt-albedo feedback. The melt-elevation feedback is a process by which the ice sheet loses mass and therefore decreases in height, but due to the higher temperature at the decreased height, the melting rate increases (Hoegh-Guldberg et al., 2018). Partially due to the melt-elevation feedback, the GIS lost $3.3 \pm 0.9\%$ of its mass due to precipitation, ice flow discharge, and meltwater runoff from 2000 to 2019 (Box, Hubbard, et al., 2022). Between 1992 and 2009, surface runoff in Greenland increased, but precipitation did not change significantly, which led to the change in surface mass balance (Rignot et al., 2011). This runoff contributes to more than half of the total mass loss in the GIS, and the increased runoff is likely to continue as the climate changes (Rignot et al., 2011). Furthermore, the melt-albedo feedback also has important implications for the GIS. This feedback occurs as surface melting exposes areas with lower reflectivity, which in turn increase the rate of melting (Box, Wehrlé, et al., 2022). In August 2021, rainfall occurred for the first time near the highest point

of the GIS as a result of an atmospheric river transporting heat and moisture poleward. As a result of this event, the GIS experienced major surface melting that was amplified by the melt-albedo feedback, and it became more pronounced since rain fell instead of snow (Box, Wehrlé, et al., 2022). If the warming climate produces more rainfall events at the GIS as opposed to snowfall, the melt-albedo feedback may therefore result in a considerable increase in melting of the ice sheet. These feedbacks can also have consequences for the stability of the GIS. There have been observations of early warning signs that the GIS is approaching a tipping point, with evidence showing that the melt-elevation feedback is the mechanism driving the destabilization of the ice sheet (Boers & Rypdal, 2021). Although previous values estimated that the GIS would experience complete melting at a global temperature increase of 3.1°C, this underestimates its sensitivity to long-term warming, and updated values estimate that complete melting will occur at around 1.6°C of warming (Robinson et al., 2012). Recent studies also suggest that certain areas of the GIS are experiencing higher melt rates than previously thought. Young et al. (2022) finds that an outlet glacier in West Greenland exhibits basal melting rates that are two orders of magnitude higher than previously estimated for an ice sheet, which indicates that the basal melting rate is comparable to the meltwater generation rate at the surface. This melting also has migrated inland toward the center of the ice sheet. The largest basin in the GIS, the Northeast Greenland Ice Stream, drains about 12% of the interior GIS and is susceptible to rapid retreat. Following the 2012 collapse of an ice shelf in the GIS, the Northeast Greenland Ice Stream experienced an acceleration in ice flow and thinning,

which has propagated more than 200 kilometers inland between 2016 and 2022 (Khan et al., 2022).

Melting in both the AIS and GIS also has implications for other aspects of the climate system that can interact with GMSLR. As the ice sheets melt, they introduce freshwater into the ocean. Increased melting from the GIS would release a large quantity of freshwater, which can slow large-scale ocean circulation currents (Martin et al., 2022). However, the ocean temperature and circulation were found to return to their initial state at the same rate that they were initially perturbed. Similarly, freshwater release from the AIS forces the climate system and can produce a range of outcomes, including the expansion of sea ice and increase in the rate of ice shelf thinning (Sadai et al., 2020). Due to the differing effects that can result from freshwater forcing, it is important to account for this process to improve climate projections (Sadai et al., 2020). Due to the complex nature of melt rates, feedbacks, and potential instabilities in the AIS and the GIS, consideration of these dynamics has an important effect on GMSLR.

1.2.3. Glaciers and Small Ice Caps

Glaciers and small ice caps (GSIC), which are smaller masses of ice distinct from ice sheets, have the combined potential to produce about 0.35 meters SLE (Cazenave & Llovel, 2010). Glaciers change sea level via mass imbalance, and their response time ranges from a few years to a few hundred years (Fox-Kemper et al., 2021). The GSIC in some mountain regions are expected to completely melt by 2100, while more dominantly glacierized areas will likely contribute to GMSLR past 2100

(Zemp et al., 2019). However, there are significant difficulties associated with global glacier modeling due to uncertainties in initial conditions, model assumptions and simplifications, and local climate conditions (WCRP Global Sea Level Budget Group, 2018). Evidence shows that mass loss from GSIC may be larger than previously reported, and in reality accounts for 25-30% of total sea level rise observed between 1961 and 2016 (Zemp et al., 2019).

1.2.4. Land-Water Storage

Land-water storage consists of surface water, soil moisture, groundwater storage, and snow, and it is caused by both anthropogenic actions and natural changes in the water cycle (Fox-Kemper et al., 2021). Anthropogenic influences to land-water storage include water impoundment via dams, groundwater depletion, land-cover and land-use change, deforestation/afforestation, wetland degradation, and lake storage changes (WCRP Global Sea Level Budget Group, 2018). The combined effects of human alterations to the environment have reduced land-water storage and thus increased the rate of sea level rise from this component (WCRP Global Sea Level Budget Group, 2018). Even so, changes in land-water storage add little to GMSLR compared to the other contributors, accounting for around 8% of GMSLR from 1971 to 2018 (IPCC, 2021). Observations for this component are extremely limited, but estimates find that land-water storage primarily impacts short-term fluctuations, not long-term trends (Cazenave & Llovel, 2010).

1.3. RCP and SSP Scenarios

Studies can estimate the contribution of each component of global mean sea level change to project GMSLR in the future. Projections of GMSLR require projections of climate change, which in turn require trajectories of anthropogenic emissions. Although the emissions pathway that will be followed in the future is deeply uncertain (Wong & Keller, 2017), different potential pathways can be used to explore resulting climate impacts. To represent potential future emissions trajectories, the Intergovernmental Panel on Climate Change (IPCC) defines scenario frameworks that involve different assumptions about future mitigation. One framework is the Representative Concentration Pathways (RCPs), which are defined by the level of radiative forcing *(W/m^2)* in the year 2100 (e.g., RCP2.6 corresponds to 2.6 W/m^2 radiative forcing in 2100) (Lee et al., 2021). Here we focus on four RCP scenarios: 2.6, 4.5, 6.0, and 8.5, with RCP2.6 corresponding to the lowest level of warming and RCP8.5 corresponding to the highest level of warming. Additional RCP scenarios have been developed in recent years, but we primarily consider these four scenarios since they have been subject to the most extensive analysis in current literature. A more recent framework is the Shared Socioeconomic Pathways (SSPs) (O'Neill et al., 2014, 2017; Riahi et al., 2017). Rather than corresponding to certain forcing values, the SSPs instead encompass different storylines of societal choices and economic futures. The RCPs and SSPs have been combined into scenarios with the notation *SSPx-y*, where *SSPx* represents the SSP scenario and *y* represents the RCP scenario (IPCC, 2022a). The IPCC assesses four priority scenarios: SSP1-2.6 (sustainable pathways), SSP2-4.5

(middle-of-the-road), SSP3-7.0 (regional rivalry), and SSP5-8.5 (fossil fuel-rich development) (Lee et al., 2021).

However, there are limitations to the RCP and SSP frameworks that can impact decision-making based on their projections. One of their major weaknesses is that the IPCC does not provide guidance about their relative plausibility, and instead states that the scenarios should be used to explore a range of potential futures (Chen et al., 2021). This can be problematic since projecting future climate impacts hinges on probability estimates for warming, and if relative likelihoods are not provided, then they will be assumed (Morgan & Keith, 2008). An individual may assume that all scenarios are equally likely, but in fact, there is debate on whether they are all plausible (Chen et al., 2021; Lee et al., 2021). For instance, given the current climate policies in place, it is improbable that the very high emissions associated with RCP8.5 or SSP5-8.5 can be realized (Lee et al., 2021; Srikrishnan, Guan, et al., 2022). Although unlikely, it is still possible to achieve these high emissions trajectories due to uncertainty in carbon-cycle feedbacks (Chen et al., 2021). Similarly, the low emissions pathways are built on assumptions that are inconsistent with current technology developments. The RCP2.6 scenario depends largely on carbon capture and storage (CCS) and assumes negative emissions beginning around the year 2070 (Meehl et al., 2012). However, the global rates of CCS deployment are much lower than assumed in the scenarios that limit warming to 1.5°C or 2°C, and CCS implementation still faces a range of technological, economic, and socio-cultural barriers (IPCC, 2022b). These two examples illustrate how the lack of guidance about scenario likelihood can lead to a misunderstanding of the feasibility of different scenarios. There are also a limited

number of scenarios that have been defined, which restricts coverage of potential future outcomes. Another limitation with the RCP and SSP scenarios is that they are only defined out to 2100, which is an insufficiently long length of time to explore the implications of climate processes that operate on at least centennial timescales, such as global ocean temperature and global mean sea level changes (IPCC, 2021). Although Extended Concentration Pathways (ECPs) ranging from the years 2100 to 2300 have been developed to explore long-term climate responses, the ECPs were generated with simple rules based on stakeholder consultations and do not represent fully consistent scenarios (Chen et al., 2021). The ECPs also further reduce the size of the scenario set from the RCP and SSP framework, resulting in even more limited coverage of future outcomes for longer-term timescales.

1.4. Linking Mitigation and Adaptation

Despite these limitations, the RCP and SSP scenarios are useful frameworks to explore potential climate futures. These scenarios can be viewed as a proxy for mitigation efforts, which can then be used to produce resulting climate impacts that require adaptation. This allows for a linkage between mitigation and adaptation, yet the two levers are often addressed separately and viewed as different problems (Martens et al., 2009). This separation is partially due to the different spatiotemporal scales on which mitigation and adaptation operate, as well as a different array of stakeholders involved in the two levers (Martens et al., 2009). Although these characteristics present challenges to linking mitigation and adaptation, connecting them is important since their actions have an impact on each other via the climate

change feedback loop (see Figure 1). Several studies attempt to bridge this gap between the two levers. To examine the role of mitigation choices in impacting future climate and economic outcomes, Lamontagne et al. (2019) conducts a sensitivity analysis of the impacts of uncertain socioeconomics and abatement decisions using an economic model. The study finds that although present mitigation does not alleviate near-term warming, it is the primary driver of long-term warming, and the value of climate sensitivity heavily dictates future climate damages and therefore adaptation needs (Lamontagne et al., 2019). However, one limitation of this study is the use of an aggregate climate damage function as a proxy for climate impacts, which represents climate damages as a percentage of the gross world product. Since climate damages is an aggregated metric, it does not allow for disaggregation into specific climate impacts, such as temperature or GMSLR. This prevents an analysis of individual climate impacts, which in turn inhibits understanding of climate risks.

Rather than using an aggregated representation of climate impacts, various other studies use the RCPs and SSPs to examine specific climate risks. Rohmer et al. (2021) uses the SSP-RCP framework to represent mitigation, and the study examines the resulting adaptation required to manage coastal flood risks. They explore coastal flooding using two risk metrics: expected annual damage and adaptation costs. Using random forests and a variance-based global sensitivity analysis, they analyze how the drivers of uncertainty in the two metrics change over time. They find that prior to 2040, modeling uncertainties drive the uncertainty in expected annual damage, but in the long-term, the uncertainty is primarily controlled by the uncertainty in the SSP scenario. For adaptation costs, regional sea levels primarily control uncertainty before

2050, but after that, the choice of RCP scenario is the main driver of uncertainty (Rohmer et al., 2021). This implies that more aggressive mitigation reduces uncertainty in adaptation costs. Similarly, Hough & Wong (2022) explores coastal flood risk as a result of the RCP scenarios, but the study instead focuses on specific characteristics of the Earth system that drive risk. They use two radiative forcing scenarios (RCP2.6 and RCP8.5) to identify which Earth system parameters in an ice sheet model dominate global mean sea level through 2100. By constructing random forests for RCP2.6 and RCP8.5 that focus on high-end sea level scenarios, they determine that the components of climate sensitivity and the aerosol scaling factor have the most influence on outcomes (Hough & Wong, 2022). They also find that thermal expansion primarily drives coastal flood risk in the near-term, but melting from the AIS and the GIS is the dominant driver of hazards in the long-term. Lastly, Nauels et al. (2017) also explores coastal flood risks by examining how socioeconomic drivers of emissions and radiative forcing targets impact GMSLR. Using the SSP framework and a sea level emulator coupled with a simple carbon-cycle model, they estimate GMSLR under many combinations of radiative forcing targets and socioeconomic pathways. They find that GMSLR estimates and socioeconomic indicators, such as population growth and gross domestic product, vary widely among the SSPs (Nauels et al., 2017). An important caveat of the latter three studies is their use of the SSP/RCP framework. As discussed previously, a major limitation of this framework is that there are only a small number of pre-defined scenarios with no guidance about their relative likelihood. This restricts an analysis' ability to explore other potential scenarios and assess the impact of scenario assumptions on climate

impacts. Since the RCPs and SSPs are only defined until 2100, their limited timeframe also prevents exploration of climate impacts on centennial timescales.

Therefore, previous studies primarily explore the interactions between uncertain mitigation pathways and the uncertain Earth system response using deterministic, pre-defined emissions scenarios. To address these limitations in previous work, we create an ensemble of emissions trajectories through 2300 that allows for flexibility in combinations of emissions growth rate, year of peak emissions, and decarbonization rate. The structure of the emissions curves enables examination of specific aspects of an emissions trajectory that drive variability in future climate impacts. The longer timeframe facilitates exploration of long-term processes that operate on centennial timescales, such as GMSLR. Since a particular environmental pathway (i.e., temperature goal) can be achieved with a variety of different storylines for energy and technology development (Morris et al., 2022), we generate emissions curves directly rather than using socioeconomic drivers to produce trajectories. This allows for exploration of a range of potential futures that could produce the same emissions pathway, rather than focusing on specific socioeconomic storylines. We then chain the emissions trajectories to an Earth system model and an ice sheet model to produce GMSLR. Therefore, we use a range of flexible emissions trajectories instead of discrete scenarios (as in previous studies) to account for mitigation uncertainty, and we use these emissions pathways to explore resulting climate impacts. Using this framework, we examine three key questions: (1) To what extent do different emissions pathways alleviate future climate impacts?, (2) What are

the most influential drivers of variability in global mean sea level rise?, and (3) To what extent do these drivers vary over time?

2. METHODS

2.1. Workflow

To answer these questions, we use the emissions trajectories to force a coupled Earth system model (SNEASY) and ice sheet model (BRICK), producing associated series of GMSLR. Given the input of emissions, SNEASY models the carbon cycle and climate system to transform the emissions into a concentration and then a radiative forcing, producing an output of ocean heat and global mean temperature. This output from SNEASY is used as the input to BRICK, which models the sea level response to the forcing from SNEASY. BRICK then produces the final output of global mean sea level. This model chain is shown in Figure 2.

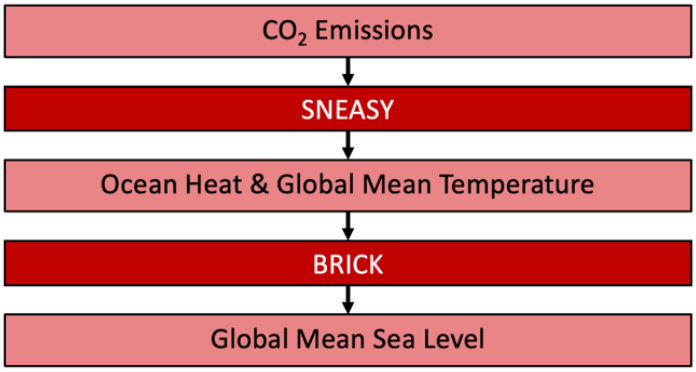

Figure 2. Flowchart of model inputs and outputs.

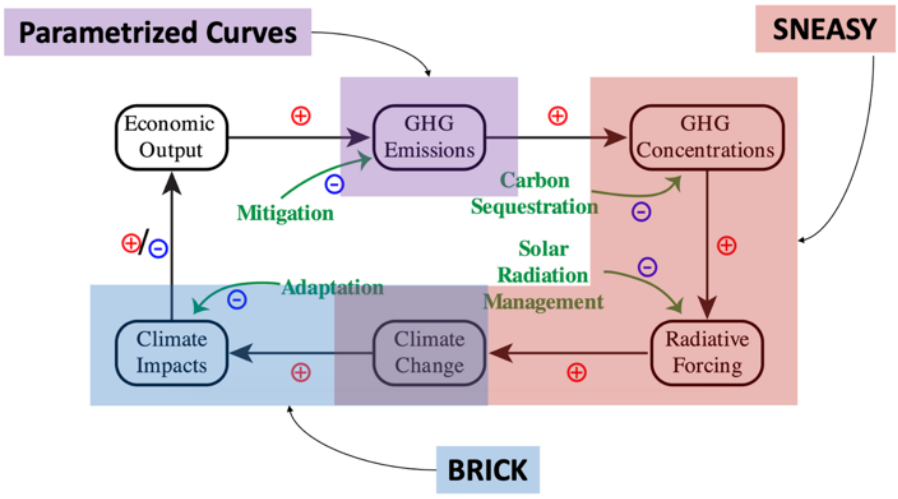

Figure 3. Integration of workflow components into broader climate feedback framework.

By progressing through each stage of the workflow, we move through the different components of the climate feedback loop (Figure 3). Notice that we start with the emissions component rather than the economic output component. This is because we do not account for the socioeconomic drivers of the emissions pathways, but rather we consider the trajectories themselves. SNEASY then models the next three stages before producing the climate change outputs of ocean heat and temperature. BRICK overlaps with SNEASY to cover the final two stages of climate change and climate impacts.

Through each stage of the climate feedback loop, additional uncertainties compound in the model output (Figure 4). To visualize these compounding uncertainties, we select three CO_2 trajectories that represent low, medium, and high levels of emissions. These trajectories roughly correspond to 2.4, 4.7, and 6.8 W/m^2 of radiative forcing in 2100, respectively. In Figure 4a, the emissions trajectories are deterministic and do not include uncertainty. Figure 4b contains slightly more

uncertainty due to carbon-cycle uncertainties, Figure 4c includes additional uncertainties from the climate system, and Figure 4d contains the full range of uncertainties with the inclusion of the uncertainties in thermal expansion, ice sheets, glaciers and small ice caps, and land-water storage (for an explanation of the change in radiative forcing behavior past 2200 in Figure 4b, see Appendix A). Figure 4d illustrates the large total uncertainty in GMSLR projections in the year 2300, which shows considerable overlap between the medium and high emissions pathways. However, the low emissions trajectory has a much smaller range of GMSLR outcomes. This underscores the idea that aggressive mitigation in the near-term reduces the risks stemming from uncertainty in Earth system processes, which have a large impact on future climate projections (Wong & Keller, 2017).

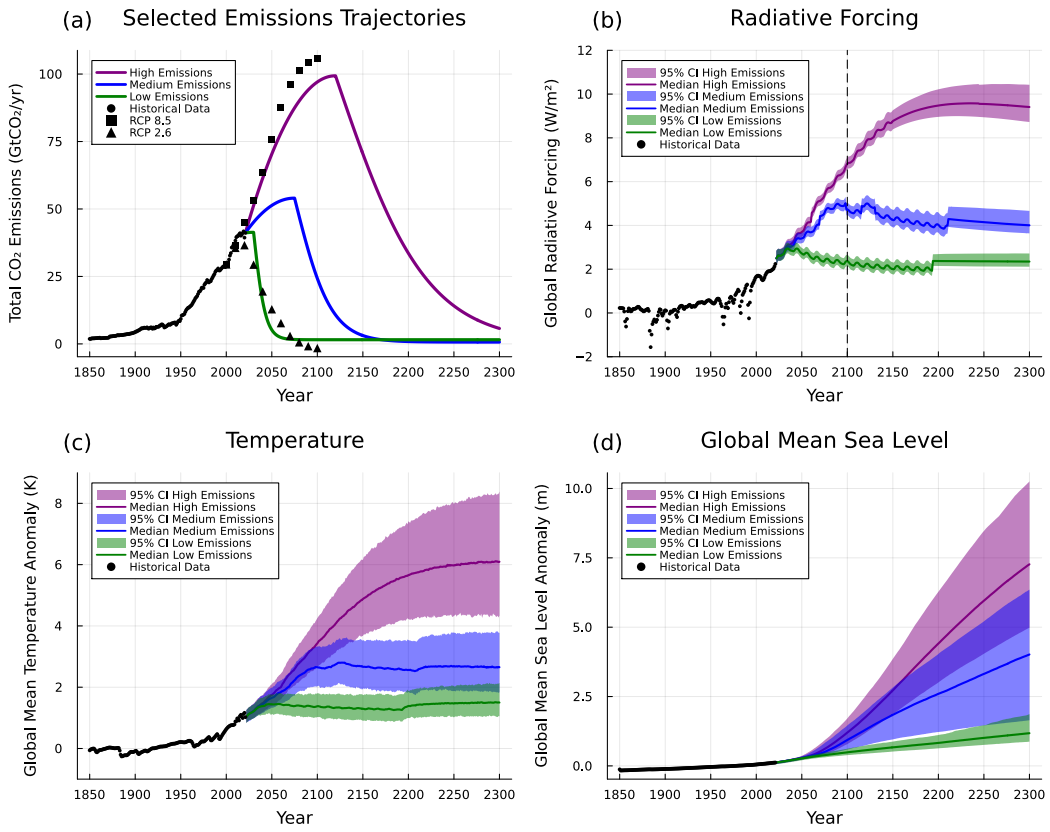

Figure 4. Compounding uncertainties through each stage of workflow.

2.1.1. Emissions Trajectories

We develop an ensemble of continuously parametrized CO_2 emissions trajectories from 2021 through 2300. Before 2021, historical observations are used. From the years 1850-2005, we use the RCP Database (International Institute for Applied Systems Analysis (IIASA), 2009), and for the years 2006-2021 we use emissions data from the Global Carbon Budget (Friedlingstein et al., 2022). We consider a single trajectory of emissions, which could be viewed as including emissions from both fossil fuel combustion and land-use change.

Each emissions trajectory is defined by three parameters: growth rate *(γ_g)*, peaking time *(t_{peak})*, and decline rate *(γ_d)*. The growth rate is the rate at which CO_2 emissions continue to increase, the peaking time is the year at which CO_2 emissions reach a maximum value, and the decline rate is the rate at which decarbonization occurs. Prior to and including the peaking year, the quantity of carbon dioxide emissions increases quadratically, and after the peaking year, the emissions decrease logistically. Following the model of quadratic growth and logistic decline, the emissions trajectories are defined by the following piecewise function:

$$q(t) = \begin{cases} q_{t-1} + \gamma_g\left(t_{peak} - t\right) & if \quad t \le t_{peak} \\ q_{t-1} - \left[\frac{2q_{t_{peak}} * \gamma_d * \exp\left(\gamma_d\left(t - t_{peak}\right)\right)}{\left[\exp\left(\gamma_d\left(t - t_{peak}\right)\right) + 1\right]^2}\right] & if \quad t > t_{peak} \end{cases} \tag{1}$$

where *q(t)* is the quantity of carbon dioxide emissions *($GtCO_2$)* at time *t*, q_{t-1} is the quantity of carbon dioxide emissions *($GtCO_2$)* at the previous timestep, t_{peak} is the peaking year for an individual sample, and q_{tpeak} is the quantity of carbon dioxide emissions *($GtCO_2$)* at t_{peak} for that sample. Each of the three parameters are defined by a truncated normal *(TN)* distribution with the notation $TN(\mu, \sigma, a, b)$, where μ represents the mean, σ represents the standard deviation, and *a* and *b* represent the lower and upper bounds of the truncated distribution, respectively. The bounds are inclusive apart from the upper bound of infinity in Equation (2).

$$\gamma_g \sim TN(0.004,\ 0.0075,\ 0.001,\ Inf) \tag{2}$$

$$t_{peak} \sim TN(2070,\ 25,\ 2030,\ 2200) \tag{3}$$

$$\gamma_d \sim TN(0.07,\ 0.05,\ 0.001,\ 0.2) \tag{4}$$

To illustrate how the piecewise function and parameter distributions translate into emissions curves, we randomly generate a selection of emissions trajectories to demonstrate their behavior (Figure 5). These curves represent a range of possible emissions pathways that may be realized in the future. We design the trajectories to encompass a range of potential emissions bounded by the extreme IPCC scenarios: RCP2.6 and RCP8.5 (Figure 6) (see Section 1.3). It is important to note that we avoid the assumption of negative emissions, so the trajectories here cannot decline below zero due to the structuring of the logistic decline. We make this choice because the potential role of negative emissions technologies is deeply uncertain, and a consensus has not been reached on which technologies may penetrate in the future, the timeframe on which they may penetrate, and the quantity of negative emissions that may result (Srikrishnan, Guan, et al., 2022). Due to these factors, we exclude negative emissions to limit the degrees of freedom in our analysis and avoid potentially unrealistic representations of negative emissions in the trajectories.

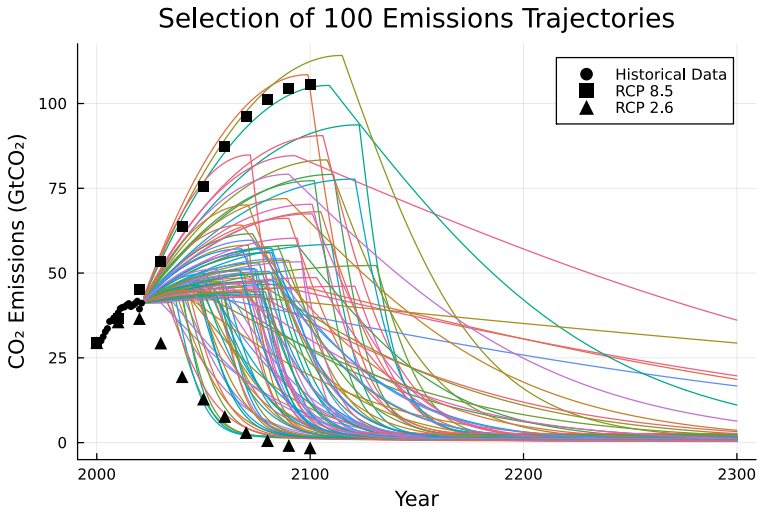

Figure 5. Selection of 100 trajectories depicting quadratic growth of emissions prior to the peaking year and logistic decline of emissions after the peaking year.

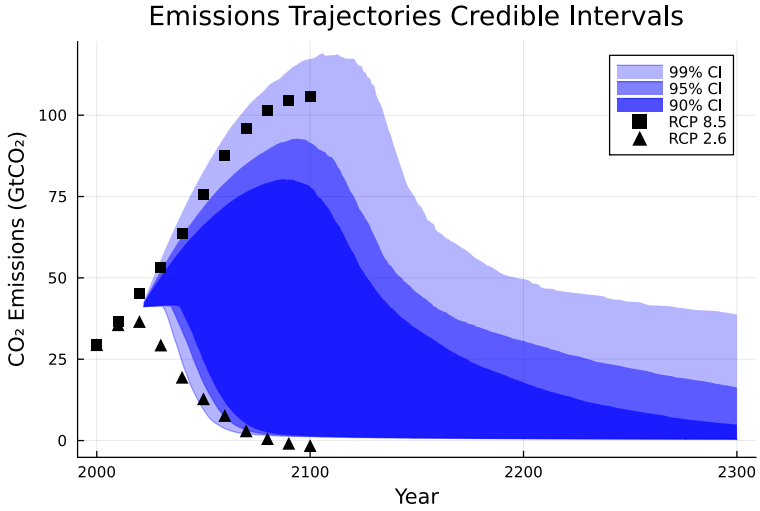

Figure 6. Credible intervals for the ensemble of generated CO_2 emissions trajectories.

Although we do not consider negative emissions here, assumptions for negative emissions are incorporated into RCP2.6, which is the reason that the credible intervals in Figure 6 do not reach the lower values in the scenario. RCP2.6 also has a peaking time prior to 2030, which is the minimum peaking year that we allow.

Because of this, the range of emissions trajectories do not decline as early as in RCP2.6, although the decarbonization rate in some trajectories is quick enough to keep pace with the emissions reductions in RCP2.6 after 2030. Conversely, the emissions trajectories do reach the full extent, and beyond, of RCP8.5. As previously discussed (see Section 1.3), there is debate on whether RCP8.5 is plausible based on the current climate policies in place (Lee et al., 2021), but we choose to include this upper extent to avoid ruling out low-likelihood, extreme outcomes and to explore the consequences of unabated emissions. Evidence also shows that the RCP scenarios underestimate the emissions and potential impacts associated with land-cover and land-use changes (Mahowald et al., 2017). Because of this, exploring trajectories with emissions slightly higher than RCP8.5 may help to account for this underestimation. Only around one percent of the emissions trajectories that we develop reach to and beyond RCP8.5, so this choice is only represented in a very small number of samples.

Furthermore, the RCPs include assumptions about non-CO_2 GHG gases and non-CO_2 radiative forcing, whereas the trajectories that we consider only represent CO_2 emissions. Since translating emissions to radiative forcing requires assumptions about non-CO_2 GHG gases, we make use of the assumptions in the RCPs. For each year in each emissions trajectory, we identify the RCP scenario that most closely matches the emissions for that SOW, and we use its value for nitrous oxide concentration in the Earth system model. To represent total radiative forcing, CO_2 forcing must be summed with non-CO_2 forcing, which includes aerosol forcing and forcing from other sources. We use the same method to match the non-CO_2 forcings

with the closest RCP scenario, and we then update the values in the Earth system model.

Using these trajectories and the updated values in the Earth system model, we generate corresponding global mean sea levels, and we then conduct a global sensitivity analysis (see Section 2.2) to identify the most influential contributors to variability in GMSLR. We run two sets of sensitivity analyses: one for the full range of emissions trajectories and the other for smaller ranges of emissions. The latter involves grouping the sampled emissions trajectories into subsets to explore key parameter sensitivities and interactions under particular assumptions about when emissions peak. The goal of this grouped sensitivity analysis is to keep the original parameter distributions intact as much as possible while examining additional Earth system sensitivities that may have been dwarfed by t_{peak} and other emissions parameters during the full ensemble sensitivity analysis. Although the growth rate and decline rate are important indicators of mitigation progress as well, we use peaking time as the primary proxy for climate mitigation ambition. Three groups are used for the grouped sensitivity analysis: "early" peaking, "middle" peaking, and "late" peaking. We define early peaking as at least the year 2030 and before the year 2050, middle peaking as at least the year 2050 and before the year 2100, and late peaking as at least the year 2100 and before the year 2200. The distributions used for t_{peak} in each of the three groups are as follows:

$$t_{peak(early)} \sim TN(2070,\ 25,\ 2030,\ \mathbf{2050}) \quad (5)$$

$$t_{peak(middle)} \sim TN(2070,\ 25,\ \mathbf{2050},\ \mathbf{2100}) \quad (6)$$

$$t_{peak(late)} \sim TN(2070,\ 25,\ \mathbf{2100},\ 2200) \quad (7)$$

The lower bounds in the peaking group distributions are inclusive, whereas the upper bounds are exclusive. The numbers in bold highlight values that deviate from the original t_{peak} distribution from Equation (3), which has a lower and upper bound of 2030 and 2200, respectively.

2.1.2. SNEASY-BRICK

We use two coupled models to generate GMSLR. The first is the Simple Nonlinear Earth System model (SNEASY), an Earth system model composed of a carbon-cycle model and a climate module (Urban & Keller, 2010). The second model is Building blocks for Relevant Ice and Climate Knowledge (BRICK), an ice sheet model that produces outputs of regional sea levels and global mean sea level (Wong, Bakker, Ruckert, et al., 2017). We run the coupled SNEASY-BRICK over the years 1850-2300 to produce series of global mean sea level, which are reported as an anomaly relative to the 1986-2005 mean.

SNEASY involves a carbon-cycle model and a simple representation of the climate system (Urban & Keller, 2010). The climate module uses an energy balance model composed of an atmospheric and oceanic component that evaluates global temperature and ocean heat content. The uptake of heat into the interior ocean is calculated by a diffusion equation, which is used to determine the ocean heat content. Temperature changes from the climate module then impact carbon sources and sinks in the carbon cycle, which in turn affect the atmospheric CO_2 concentration. Finally, the CO_2 concentration closes the loop by forcing the climate module, and the value of climate sensitivity has a direct impact in translating the radiative forcing to a resulting

global temperature. Within the climate module, aerosols impact the amount of solar radiation that reaches the surface, thus altering the energy balance of the Earth in a process called the aerosol-forcing feedback. Interactions between aerosols and clouds, as well as indirect impacts of aerosols, contribute to considerable uncertainty in the aerosol-forcing feedback. SNEASY accounts for the uncertainty in this feedback by using an aerosol scaling factor, which is scale factor applied to the radiative forcing. A full description of SNEASY is detailed in Urban & Keller (2010).

BRICK is a computationally efficient, semi-empirical model that projects sea level change, and it has been used to assess the risk surrounding coastal flooding hazards (e.g., Hough & Wong, 2022; Ruckert et al., 2019; Vega-Westhoff et al., 2020; Wong & Keller, 2017). BRICK models sea level rise as the sum of five components:

$$\frac{dS}{dt}(t) = \frac{dS_{GSIC}}{dt}(t) + \frac{dS_{GIS}}{dt}(t) + \frac{dS_{AIS}}{dt}(t) + \frac{dS_{TE}}{dt}(t) + \frac{dS_{LWS}}{dt}(t) \quad (8)$$

where $S(t)$ is the global mean sea level *(m)* in year *t*. S_{GSIC} is the sea-level contribution from glaciers and small ice caps (GSIC), S_{GIS} is the sea-level contribution from the Greenland Ice Sheet (GIS), S_{AIS} is the sea-level contribution from the Antarctic Ice Sheet (AIS), S_{TE} is the sea-level contribution from thermal expansion (TE), and S_{LWS} is the sea-level contribution from land-water storage (LWS). All five components use units of meters. BRICK also includes a representation of rapid AIS dynamics and MISI, as well as inclusion of feedbacks such as the feedback between sea level change and the behavior of the AIS (Helgeson et al., 2021). For the rapid AIS dynamics, the model incorporates a surface temperature threshold for the ice sheet. BRICK assumes that below this threshold, the AIS is stable, and above this threshold, the ice sheet is vulnerable to fast disintegration.

The implementation of SNEASY-BRICK used here (MimiBRICK.jl) is written in the Julia programming language. Both SNEASY and BRICK are in the Mimi integrated modeling framework, which is a coding platform that facilitates model coupling and running experiments with coupled models (Wong et al., 2022a). We use prior results from a Bayesian calibration approach for SNEASY-BRICK to resolve the tails of the distribution of sea level rise (Wong et al., 2022b). The calibration considers the full parameter set with observational constraints, which allows for a representation of correlations, such as those between climate sensitivity, ocean heat uptake, and aerosol scaling. The calibration is described in detail in Wong, Bakker, Ruckert, et al. (2017), but we cover relevant aspects and parameter distributions in Appendix B.

2.2. Sensitivity Analysis

We conduct a global sensitivity analysis (GSA) on the model chain to examine the influence of uncertainty of the model parameters on GMSLR. A key advantage of a GSA is that it explores the entire feasible parameter space, whereas a local sensitivity analysis does not (Reed et al., 2023). A GSA can also identify relevant parameter interactions that would otherwise be overlooked with a local sensitivity approach (Oddo et al., 2020). However, a global approach can be infeasible for more complex models, which are computationally expensive and thus have a longer run time (Saltelli, 2002) (see Section 1.1). This reiterates the motivation for the model selection of SNEASY-BRICK, which has a sufficiently fast run time to make a GSA computationally feasible.

We use the Sobol' method (Saltelli et al., 2008; Sobol′, 2001), a variance decomposition method for a global sensitivity analysis. To explore the influence of each sea-level contributor on the simulated GMSLR output, we categorize the input factors into nine distinct groups: Antarctic, carbon cycle, climate system, emissions, glaciers and small ice caps, Greenland, land-water storage, thermal expansion, and model discrepancy/observational error (called "statistical noise" parameters going forward). The Antarctic group encompasses both the Antarctic Ice Sheet and the Antarctic Ocean parameters, whereas the Greenland group only consists of the Greenland Ice Sheet. By creating different categories, we can identify which group of parameters contributes to the most variance in the output of GMSLR over different timescales.

The Sobol' method can calculate a parameter's individual influence (first-order index), its influence from interacting with other parameters (higher-order indices), and its total influence (total-order index) on an output. Higher-order sensitivities include interactions between two parameters (second-order), three parameters (third-order), etc., but low-order interactions among parameters typically have the largest impact on the output (Sobol′, 2001). Because of this, we only examine first-, second-, and total-order sensitivities in our analysis. The first-order sensitivity index (S_i^1) indicates the output variance explained by an individual input factor, while the second-order sensitivity index $(S_{i,j}^2)$ indicates the output variance explained by the interactions between two input factors. The total-order sensitivity index (S_i^T) represents the entire influence of an individual input factor on the output variance, including its individual contribution and all its interactions with other factors. The first-, second-, and total-

order sensitivities are obtained with the following three equations (Reed et al., 2023), respectively:

$$S_i^1 = \frac{V_{x_i}[E_{x\sim i}(x_i)]}{V(y)} \tag{9}$$

$$S_{ij}^2 = \frac{V_{x_{i,j}}[E_{x\sim i,j}(x_i,x_j)]}{V(y)} \tag{10}$$

$$S_i^T = \frac{E_{x\sim i}\left[V_{x_i}(x_{\sim i})\right]}{V(y)} = 1 - \frac{V_{x\sim i}\left[E_{x_i}(x_{\sim i})\right]}{V(y)} \tag{11}$$

where E represents the expected value, V represents the variance, x_i denotes an input factor, and $x_{\sim i}$ represents all input factors except for x_i.

To conduct the sensitivity analysis, we use the implementation of the Sobol' method in GlobalSensitivity.jl, a Julia package for GSA (Dixit & Rackauckas, 2022). We generate design matrices for the parameters using a quasi-Monte Carlo sampling scheme. For the three emissions parameters (growth, peaking, and decline), we sample uniformly between 0 and 1 to generate an ensemble of percentiles. We then sample the percentiles over the corresponding distributions for each parameter to produce an ensemble of emissions samples. For the Earth system and statistical noise parameters, we use the results of the SNEASY-BRICK calibration, which was conducted using Markov chain Monte Carlo (MCMC) (see Appendix B for details). We then concatenate the emissions samples and the Earth system samples to produce design matrices for the full ensemble GSA. We run the GSA from 2030-2300, computing the first- and total-order indices every 10 years, and the second-order indices every 50 years. Using the same approach, we conduct grouped sensitivity analyses for early, middle, and late peaking times (defined in Section 2.1.1), with the only difference being the distribution specified for the peaking time.

3. RESULTS

3.1. Climate Projections

After running the chain of models for the full ensemble of samples, we use the resulting radiative forcings, temperatures, and GMSLR to examine future climate impacts. For each of the three climate outcomes, we categorize the results into different groups of emissions peaking time to determine how different levels of mitigation ambition alter climate projections. To do this, we establish indices for SOWs with early, middle, and late peaking times, which we define using the same lower and upper bounds as described in Section 2.1.1. Using these groups as a frame of reference, we analyze how the three climate outcomes (radiative forcing, temperature, and GMSLR) and contributors to GMSLR vary by peaking group and time period.

There are uncertainties in both the emissions pathways and Earth system dynamics that interact to produce larger uncertainties over time, which results in wider distributions for radiative forcing, temperature, and GMSLR as time progresses (Figure 7). For emissions, the values of peaking time, growth rate, and decline rate interact to determine the cumulative emissions for each trajectory. For trajectories that peak quickly, the decline rate has more of an influence on cumulative emissions uncertainty than the growth rate since there is more time for varying decline rates to alter emissions. The reverse applies as well: for trajectories with delayed peaking, the growth rate is more important in determining the cumulative emissions produced. In the middle peaking group, both cases apply since the growth rate and decline rate both have sufficient time to impact emissions, which causes the middle group to have the

widest range of cumulative emissions. The late group has the second-highest variation in cumulative emissions since the trajectories have plenty of time to grow at different rates and diverge from each other. Conversely, trajectories that peak early have limited time to grow, so variation in the decline rate in the early peaking group contributes less to variation in cumulative emissions than it does in the middle and late peaking groups. Due to this smaller range of cumulative emissions in the early peaking group, the Earth system risks are reduced and thus cause the three climate outcomes in Figure 7 to exhibit a smaller interquartile range compared to the middle and late groups.

Once emissions approach zero, GHG concentrations in the atmosphere begin to level off and therefore lead to stable radiative forcings and temperatures. In the early and middle peaking groups, emissions must reach their maximum and begin to decline prior to 2050 and 2100, respectively, after which radiative forcing and temperature can begin to slow their rate of increase. However, these outcomes will not stabilize under continued emissions. Since the emissions in the late group cannot peak until 2100 at the earliest, radiative forcing and temperature will continue to increase past 2100. Additionally, there is a lag between the peaking time of emissions and a reduction in atmospheric concentration, which is due to the very long lifetime of CO_2 in the atmosphere (Lee et al., 2021). Due to this long lifetime, CO_2 concentrations, as well as the resulting radiative forcings and temperatures, will not begin to decline immediately after emissions peak, but they will instead gradually decline on longer timescales. Because of this time lag, the lower end of the radiative forcing and temperature distributions begins to decline slightly through time. This decline happens

sooner in the early peaking group and is more delayed in the late peaking group due to the different timeframes that emissions begin to decrease in the groups.

Even after radiative forcing and temperature stabilize, however, there are continued changes in ocean temperatures as warmer air mixes with the upper ocean and then mixes in increasingly deep ocean regions (Meehl et al., 2012). Because of this, the ocean temperature responds to atmospheric forcing on a longer timescale than the air temperature, leading to higher GMSLR even after emissions reach zero. This is illustrated in Figure 7, where median GMSLR increases steadily from 2100 to 2300 for all groups. This is consistent with the work of Meehl et al. (2012), which finds that under the RCP2.6 scenario (i.e., low emissions), global temperature levels off by 2100 and then begins to decline, but global mean sea level continues to rise after 2100. This behavior highlights the slower response time of the ocean to emissions changes compared to radiative forcing and temperature, making it more difficult to stabilize GMSLR.

For each peaking group, we examine the SOW with the maximum global mean sea level anomaly, which serves as a proxy for worst-case climate risks posed by GMSLR. In 2300, the maximum sea level anomaly is approximately 9 meters for the early group, 11 meters the middle group, and 13 meters for the late group (Figure 7i). The cumulative emissions that drive these outcomes are also progressively larger for each peaking group, with a value of around 12,000 $GtCO_2$ for the early group, 18,000 $GtCO_2$ for the middle group, and 25,000 $GtCO_2$ for the late group. All values for cumulative emissions are extreme, falling at >99^{th} percentile in their respective groups. The SOWs with maximum GMSLR are also accompanied by high climate

sensitivities (>92nd percentile for all groups), which result in extreme temperature outcomes (>99th percentile for all groups). Although these maximum values represent low-likelihood events, the enormous magnitude of projected sea level change highlights the extreme risks posed by GMSLR.

Even neglecting extreme outliers, GMSLR outcomes are sufficiently high to necessitate adaption regardless of peaking group, and even rapid mitigation cannot fully manage the risks posed by sea level rise. Under an early peaking group, the median GMSLR in 2100 is 0.61 meters, with a 75th percentile of 0.72 meters (Figure 7g). Closer to present day in 2070, the median GMSLR is 0.41 meters (Figure C-1), even though emissions peak prior to 2050 for this group. By 2070, a GMSLR of 0.41 meters still poses substantial climate risks and adaptation needs. The IPCC estimates that if global mean sea level increases by 0.15 meters, the population potentially exposed to a 100-year coastal flood will increase by around 20%, and the exposed population will double at 0.75 meters and triple at 1.4 meters, assuming no additional adaptation or population change (IPCC, 2022a). This estimate has concerning implications about future climate risks, especially since the median value for the early peaking group increases further to 1.55 meters in 2300, with a 75th percentile of 2.16 meters (Figure 7i). Despite assuming early peaking, both of these values fall above the highest GMSLR considered in the IPCC estimate, thus exposing a large number of people to heightened coastal flood risks. As a result, even if emissions peak over the next few decades, adaptation measures will be required to manage GMSLR-driven risks.

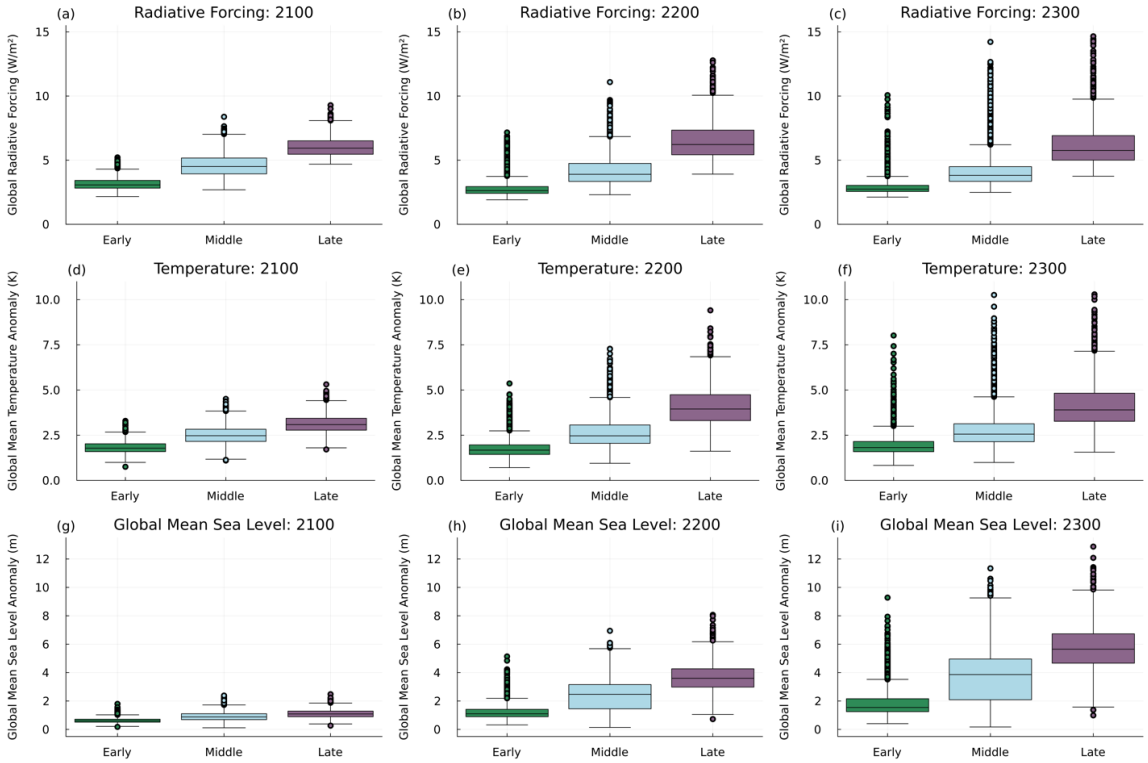

Figure 7. Radiative forcing, temperature, and GMSLR outcomes across peaking groups and years.

To better understand the risks posed by GMSLR, it is important to examine the processes behind two of its major contributors: the Greenland and Antarctic Ice Sheets. BRICK models the GIS as melting approximately linearly with temperature increase, while AIS dynamics involve tipping points which accelerate its contribution to GMSLR, increasing uncertainty (Figure 8). This is reflected in the BRICK equations for volume change in the AIS and the GIS, respectively (Wong, Bakker, Ruckert, et al., 2017):

$$\frac{dV_{AIS}}{dt}(t) = B_{tot}(T_A, R) + F(S, R) \tag{12}$$

$$\frac{dV_{GIS}}{dt}(t) = \frac{1}{\tau_{GIS}(t)}\left(V_{eq,GIS}(t) - V_{GIS}(t)\right) \tag{13}$$

In Equation (12), dV_{AIS} is the Antarctic Ice Sheet volume *(m^3)*, B_{tot} is the total rate of accumulation of mass on the AIS (*m^3/yr)*, T_A is the Antarctic surface temperature reduced to sea level *(℃)*, *R* is the AIS radius *(m)*, *F* is the ice flux at the grounding line *(m^3/yr)*, and *S* is the sea level *(m)* (Wong, Bakker, Ruckert, et al., 2017). In this formulation, the second term, *F(S,R)*, includes the accelerated melting of the AIS upon passing a temperature threshold. If the specified critical temperature is reached, then the ice flux at the grounding line increases. In Equation (13), dV_{GIS} is the Greenland Ice Sheet volume *(m^3)*, τ_{GIS} is e-folding timescale of GIS volume changes due to changes in global temperature (*yr^{-1})*, and $V_{eq,GIS}$ is the equilibrium ice sheet volume at which the sea-level contribution from the GIS is zero *(m sea-level equivalent)* (Wong, Bakker, Ruckert, et al., 2017). The sea level rise of the GIS is therefore a result of the change from the initial GIS volume to the current volume, and this change occurs as a direct response to the change in temperature that the GIS experiences. Due to the different representations of volume change for the two ice sheets, the AIS can experience rapid melting, whereas the GIS melting is primarily controlled by temperature changes.

Although the AIS generally melts more with increasing temperature, the uncertainty involved in its threshold response causes the samples to spread out and deviate from a linear relationship (Figure 8a-c). The tipping point of the AIS may or may not be triggered depending on the emissions pathway and temperature threshold for a particular SOW. Trajectories with early peaking and lower cumulative emissions are less likely to trigger fast melting dynamics, whereas late peaking and higher cumulative emissions are more likely to trigger it. Although early peaking and lower

cumulative emissions are less likely to activate the tipping point, this is not always the case. Depending on the emissions curve and Earth system characteristics (specifically those in the carbon cycle, climate system, and Antarctica) for a specific SOW, the Antarctic tipping point may be triggered and therefore lead to substantial GMSLR. Figure 8a-c illustrates this behavior, where there are some SOWs where the AIS fast melting dynamics are triggered with small temperature increases. The inverse is true as well, with some SOWs showing little melting of the AIS in response to large temperature increases, highlighting the importance of climate system and Antarctic uncertainties in determining melting outcomes. As discussed above, the smaller range of cumulative emissions for the early peaking group constrains climate outcomes and reduces uncertain risks from the Earth system, resulting in a smaller range of temperatures and subsequent melting of the AIS and the GIS (green points in Figure 8). Due to the wider range of cumulative emissions in the middle and late peaking groups and increased potential of Earth system dynamics to substantially impact climate outcomes, these groups have a wider range of temperature and melting outcomes for both the AIS and the GIS (blue and purple points in Figure 8). Since AIS fast melting is less likely to occur in the early peaking group, high GMSLR outcomes are less likely, resulting in additional higher-end outliers for GMSLR in the 2200 and 2300 periods for early peaking than for the other two groups (Figure 7h, i). However, high GMSLR outcomes are more typical in the middle and late peaking groups due to the increased likelihood of AIS fast melting dynamics. This is evidenced by a wider interquartile range and a smaller range of upper outliers in 2200 and 2300 in the middle and late groups compared to the early group.

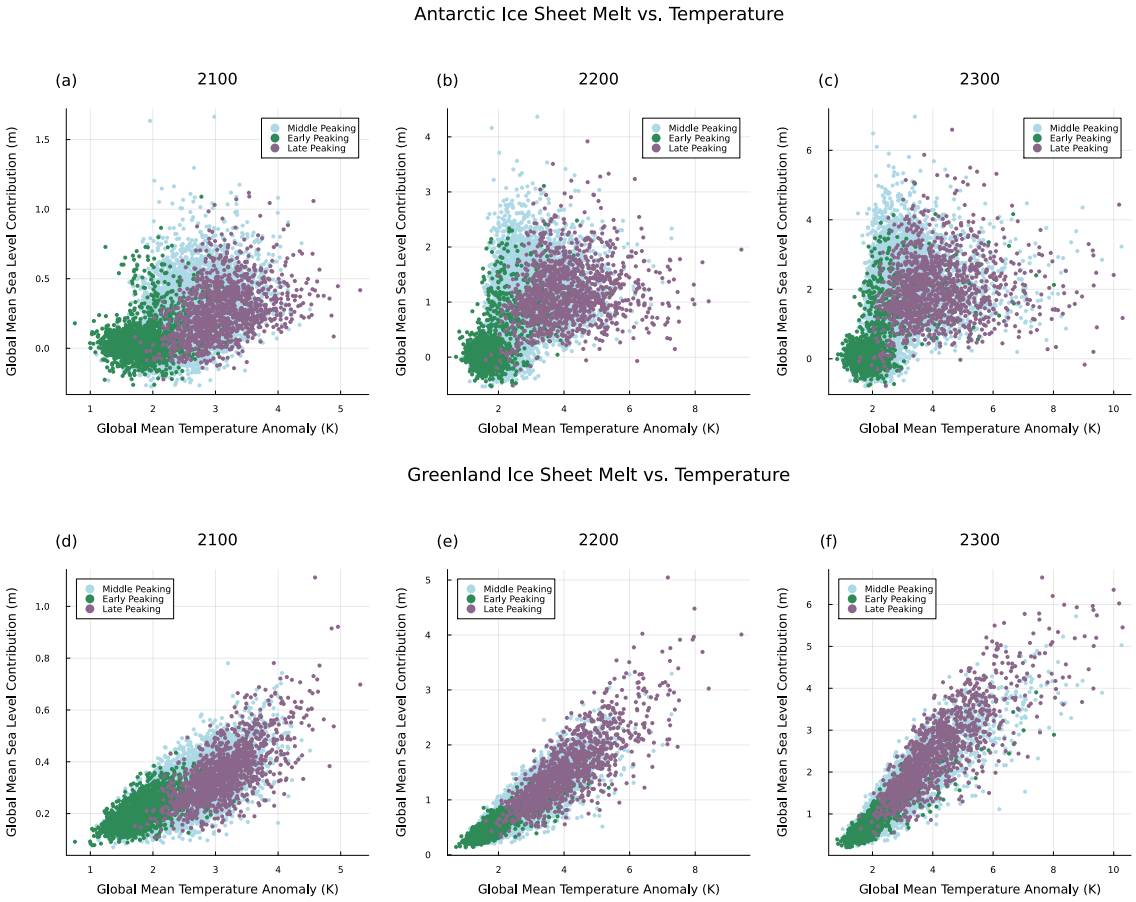

Figure 8. Antarctic and Greenland melting in response to temperature for selected years.

In addition to the AIS and GIS contributions, it is also important to consider the other components of GMSLR for a comprehensive understanding of its drivers. To analyze how differences in emissions trajectories impact sea-level contributions, we plot the components of GMSLR for each peaking group across time (Figure 9). In all years and groups, land-water storage is a minor contributor to GMSLR, which is consistent with its tendency to produce short-term fluctuations in GMSLR rather than long-term changes, as well a tendency to both increase and decrease sea level to create a canceling effect (Cazenave & Llovel, 2010). Although different peaking groups

result in different dominating contributors to GMSLR over time, the Greenland and Antarctic groups are the primary contributors in most time periods and peaking groups. These two contributors also have the most potential to produce extreme sea level rise, as evidenced by the large number of upper-end outliers in all groups and time periods. These outliers represent low-probability, high-impact outcomes such as rapid or complete melting of the ice sheets, illustrating the potential for uncertain Earth system dynamics to create extreme GMSLR from the two ice sheets under any peaking group.

To further investigate the drivers of extreme GMSLR outcomes, we examine the upper outliers for AIS melting for each peaking group in 2300 (Figure 9g-i). For the early, middle, and late peaking groups, the maximum value for the AIS contribution to GMSLR is 5.05 meters, 6.97 meters, and 6.59 meters, respectively. There are similarities that arise among the drivers of these outliers. All three samples correspond with extreme GMSLR (>99th percentile in their respective groups), which is understandable given the enormous contribution from the AIS alone. Furthermore, all three outcomes also have exceedingly high values for the Antarctic fast dynamics disintegration rate, falling at >99th percentile in all groups. Since the AIS fast dynamics are triggered in all samples, this fast rate of disintegration leads to massive, rapid melting of the AIS. However, there are differences in the temperature threshold above which fast dynamics are triggered. The temperature threshold is in the 20th percentile for the early sample, 2nd percentile for the middle sample, and 30th percentile for the late sample. A smaller percentile for the temperature threshold means that a lower temperature is required to cross it, making it is easier to trigger AIS fast

melting dynamics. Because of this, it follows that the particularly low temperature threshold in the middle sample drives extreme AIS melting. However, although the early and late samples are below the median, neither have particularly low thresholds, indicating that the warming alone in these samples is sufficiently large to trigger fast melting dynamics. This is evidenced by the cumulative emissions that drive warming, which have values of 5,818 $GtCO_2$ (90^{th} percentile) for the early group, 5,742 $GtCO_2$ (38^{th} percentile) for the middle group, and 11,843 $GtCO_2$ (77^{th} percentile) for the late group. The higher emissions in the early and late samples are sufficient to increase warming and trigger the temperature threshold in both samples despite the threshold value not being an extreme outlier. In the middle sample, on the other hand, the relatively low percentile for cumulative emissions does not contribute as much to warming, but fast dynamics are triggered regardless due the very high climate sensitivity (98^{th} percentile) and very low temperature threshold (2^{nd} percentile). Furthermore, the extreme values of AIS melting in these samples do not necessarily correspond with extreme values of Greenland melting, which fall in the 94^{th} percentile for the early sample, 70^{th} percentile for the middle sample, and 75^{th} percentile for the late sample. Although all fall above the median, the latter two are not nearly as extreme as the maximum value for AIS melting (i.e., 100^{th} percentile). This highlights the differences in BRICK representation of AIS versus GIS melting dynamics, as the fast melting dynamics in the AIS can produce extreme outcomes regardless of the temperature-dependent GIS melting. Overall, the maximum values for the Antarctic contribution in each of the three emissions groups show consistently high values for the fast dynamics disintegration rate and GMSLR. However, the samples exhibit

differences in cumulative emissions, temperature threshold, and corresponding Greenland melting, which underscores the complex interactions between emissions and Earth system processes that drive climate outcomes.

Although extreme sea levels are possible in all groups, the median values illustrate the more probable dominating contributors for each group and year. For the median outcomes in the early group (Figure 9a, d, g), Greenland and thermal expansion dominate as approximately equal contributors to GMSLR in 2100, and Greenland is the largest contributor in 2200 and 2300. For the median outcomes in the middle group (Figure 9b, e, h), Greenland is the dominant contributor in 2100, Greenland and Antarctica dominate as approximately equal contributors in 2200, and Antarctica is the dominant contributor in 2300. For the median outcomes in the late group (Figure 9c, f, i), Greenland dominates GMSLR in all three time periods. This shows that under lower-emissions pathways in the near-term, thermal expansion plays a larger role in GMSLR, but in the longer-term, the contribution from ice sheets dominates. Under higher-emissions pathways, the ice sheets dominate in all time periods. Due to the large potential of the AIS and the GIS to contribute substantially to GMSLR outcomes, characterizing the uncertainties associated with their melting is crucial to better understand future climate risks.

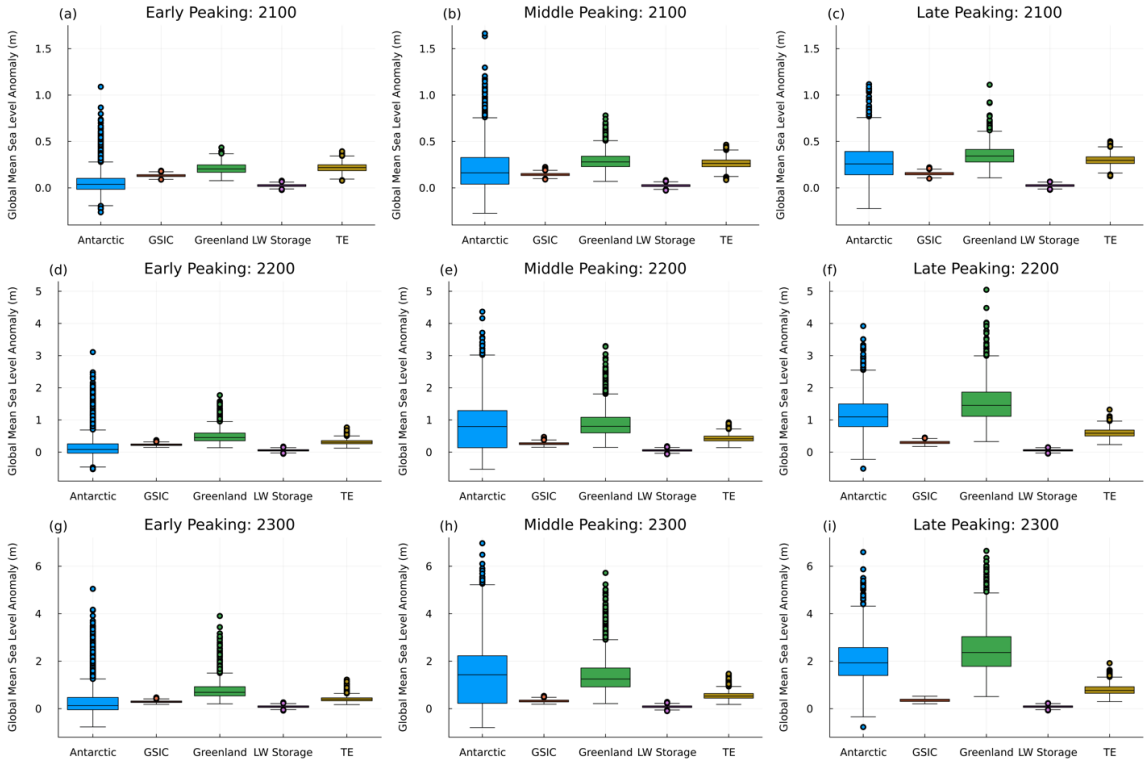

Figure 9. Contributors to GMSLR (Antarctic, glaciers and small ice caps, Greenland, land-water storage, and thermal expansion) across peaking groups and years.

To visualize how the relative contributions to GMSLR change over time in specific samples, we develop nine scenario combinations based on GMSLR and peaking groups. For GMSLR, we divide samples into different quantiles based on the global mean sea level anomaly in 2300, and we establish groups for the lowest 5% of outcomes (<5th percentile), the middle 5% of outcomes (between the 47.5th and 52.5th percentiles), and the highest 5% of outcomes (>95th percentile). These three groups are hereafter referred to as "low," "medium," and "high," respectively. For peaking time, we divide samples into the same early, middle, and late groups as discussed at the beginning of this section. Using the groups established for both GMSLR and peaking time, we combine both sets of three groups into scenario combinations, which results

in nine combinations total. The names and group characteristics for all scenario combinations are detailed in Table 1. It is important to note that there are a different number of samples that fit the criteria for each of the nine scenario combinations. For example, only one sample meets the criteria for S3 (low GMSLR and late peaking), whereas 411 samples meet the criteria for S5 (medium GMSLR and middle peaking). We select a random sample out of the total number of available samples (except in the case of S3, where only 1 sample is available). Using the one random sample for each scenario combination, we then create stacked area plots to visualize the different contributors to GMSLR over time (Figure 10). These plots do not represent uncertainty since they only show the results for one sample that meets the criteria for each scenario combination. Instead, each plot serves as an example of the behavior of a particular scenario combination and does not represent other outcomes that could be realized under a different SOW.

Table 1. Names, characteristics, and number of samples for the nine scenario combinations developed.

Scenario Combination	GMSLR Group	Peaking Group	Number of Samples
S1	Low	Early	316
S2	Low	Middle	183
S3	Low	Late	1
S4	Medium	Early	43
S5	Medium	Middle	411
S6	Medium	Late	46
S7	High	Early	7
S8	High	Middle	234
S9	High	Late	259

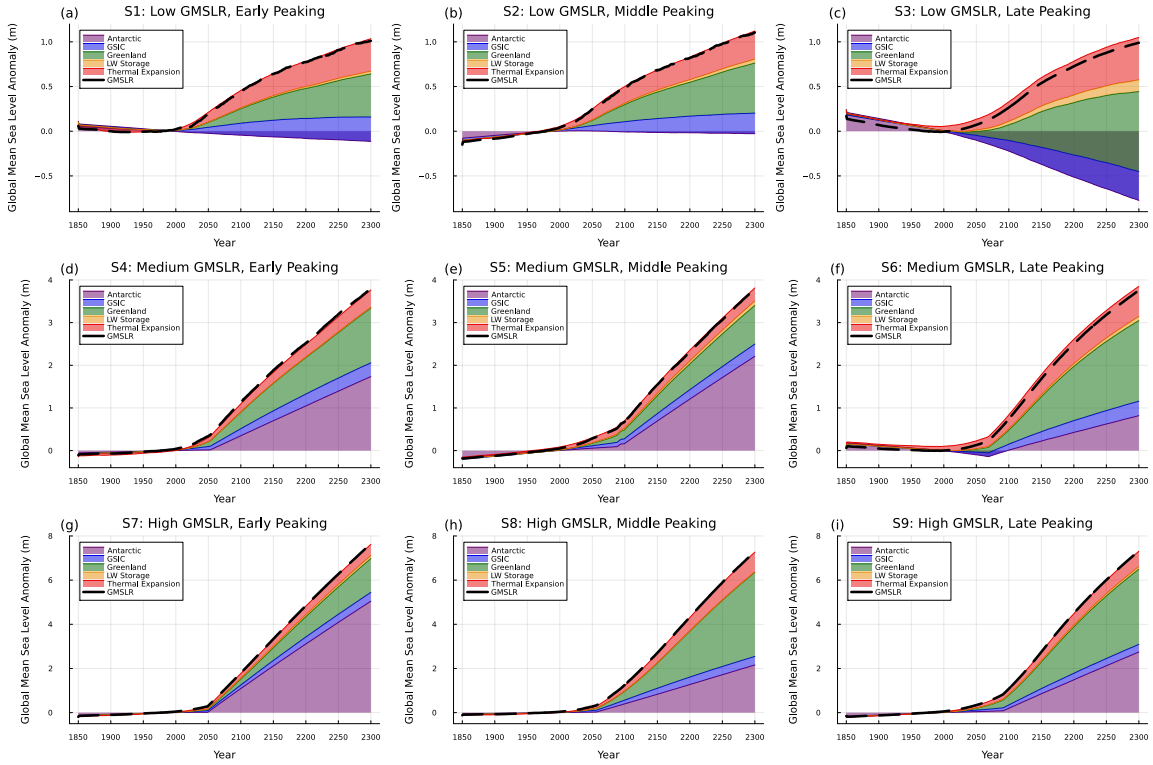

Figure 10. Changes in GMSLR contributions over time for each scenario combination.

A particular level of GMSLR can be reached with different contributions from the GMSLR components, but similarities can emerge between samples as well. In the low GMSLR scenario combinations (S1, S2, and S3; Figure 10a-c), the three samples shown result in a GMSLR of around 1 meter by 2300. The GIS dominates the change in GMSLR for the samples, followed by thermal expansion. The melting of the GIS is due to the approximately linear relationship of temperature and Greenland melting in BRICK (see Figure 8). In the early and middle peaking groups, the temperature anomaly in 2300 is 1.68 K (9^{th} percentile) and 1.49 K (4^{th} percentile), respectively, with corresponding Greenland melting of 0.48 meters and 0.56 meters. Both combinations of temperature/melting outcomes are consistent with the relationship in

Figure 8f. The contribution of thermal expansion is a result of the continued ocean warming due to its long response time, which leads to sustained thermal expansion even after emissions cease. In contrast, the AIS melting is not a major contributor in the early and middle peaking samples, which is due to the relatively high Antarctic temperature threshold (>63rd percentile for both samples). Since there is low warming in both samples, this threshold is not triggered and leads to minimal AIS melting. Notably, the late peaking group for low GMSLR (S3; Figure 10c) results in an anomalous outcome involving substantial freezing of the AIS and GSIC. However, S3 only has one available sample that meets its criteria, which reveals that this SOW is an outlier run with a very low likelihood of being realized. This is evidenced by the particularly low values in this sample for climate sensitivity (5th percentile), Antarctic Ocean temperature (4th percentile), and initial sensitivity of GSIC to surface temperature (0.55th percentile), all of which combine to produce lower warming and resistance to melting.

In the medium GMSLR scenario combinations (S4, S5, and S6; Figure 10d-f), the AIS dominates in the early and middle peaking samples, but the GIS dominates in the late peaking sample. In these three samples, properties of the climate system play a large role in determining temperatures and melting contributions. Although S4 is only in the 3rd percentile for cumulative emissions, the resulting temperature is considerably higher (46th percentile). This is because the climate sensitivity in this sample is in the 99th percentile, which creates a substantially amplified temperature increase. In all three samples, the GIS melts in response to temperature increases in S4, S5, and S6, which are in the 46th, 21st, and 77th percentiles, respectively. However,

in the middle peaking sample (S5; Figure 10e), the AIS melting is larger compared to the GIS melting due to the low temperature threshold (12th percentile) and moderately quick disintegration rate once AIS fast dynamics are triggered (64th percentile). Conversely, in the late peaking sample (S6; Figure 10f), melting in the AIS does not keep pace with Greenland despite high temperatures, which is partially due to very low values for initial sea level rise from the AIS (5th percentile) and the proportionality constant for ice flow at the grounding line (0.31st percentile). A lower proportionality constant indicates that ice flow is relatively slow and resistant to movement in response to external forces, which results in reduced ice discharge from the AIS. Because of these factors, melting from the AIS is reduced despite the higher temperatures in this sample.

In the high GMSLR scenario combinations (S7, S8, and S9; Figure 10g-i), Greenland dominates in the middle and late peaking samples due to high temperature increases. In 2300, S8 has a temperature anomaly of 5.96 K (98th percentile), and S9 has a temperature anomaly of 4.22 K (90th percentile), leading to high melting in Greenland. However, Antarctica dominates in the early peaking sample (S7; Figure 10g), whereas the Greenland melting is comparatively small. This is because this sample has lower temperatures than S8 and S9, with a temperature anomaly of 3.41 K in 2300 (78th percentile). Despite comparatively lower temperatures, the AIS fast melting dynamics are triggered in this sample, leading to an extreme amount of Antarctic melting (around 5 meters in 2300). This is because there is a relatively low temperature threshold for triggering rapid melting in this sample (23rd percentile), and once this threshold is crossed, there is an extremely high rate for Antarctic fast

dynamics disintegration (99th percentile). The sample in S7 also has cumulative emissions below the median (44th percentile), but a climate sensitivity in the 98th percentile leads to higher temperature outcomes than would otherwise result from the same level of emissions with a more moderate climate sensitivity. Due to the outlier parameter combinations in this sample, this particular SOW is one of the low-temperature, high-AIS-melting data points in Figure 8a-c. Similar to S3, very few samples fit the criteria for S7 (only 7 samples out of 10,000 SOWs), which highlights that a high GMSLR, early peaking combination requires an unlikely, unfavorable set of climate system properties and melting characteristics.

Therefore, each scenario combination shown in Figure 10 illustrates one example of how the contributors to GMSLR can change with time. Although the samples cannot be generalized to all SOWs that fit the criteria for a scenario combination, they are useful to understand how different aspects of the climate system and melting dynamics interact to determine relative contributions for each GMSLR component.

3.2. Sensitivity Analysis

3.2.1. Full Ensemble GSA

To identify the parameters that have the most influence on the variance of GMSLR throughout time, we conduct a global sensitivity analysis for the full range of peaking times from the distribution in Equation (3). We select the years 2100, 2200, and 2300 for assessment to examine how the drivers of GMSLR variability change in the long-term, which is particularly important given that GMSLR operates on at least

centennial timescales. We divide the parameters considered into groups depending on whether they are associated with emissions or different parts of the Earth system response. The parameter groups are Antarctic, carbon cycle, climate system, emissions, glaciers and small ice caps, Greenland, land-water storage, statistical noise, and thermal expansion. We consider both the first- and total-order sensitivity indices to examine both the direct impact of a parameter group itself as well as how its interactions with other parameters influence the output variance. Regarding first-order sensitivities, we find that in all time periods, emissions dwarf the impact of Earth system processes on GMSLR, and peaking time is the most influential parameter in all time periods (Figure 11). This follows from the large influence of the emissions pathway in determining climate outcomes (as described in Section 3.1), and it is also consistent with the work of Rohmer et al. (2021), which finds that uncertainty in future coastal flood risk is primarily driven by uncertainty in human activities and mitigation choices.

Out of the three emissions parameters, peaking time dominates since it has the largest impact on the cumulative amount of CO_2 that is emitted into the atmosphere. Although peaking time is by far the most important parameter in all three time periods in Figure 11, the growth rate and decline rate of emissions still play an important role. As many samples of emissions continue to grow in 2100, the growth rate of emissions continues to have a larger influence, but once all emissions have peaked by the upper bound of 2200, the growth rate is no longer as influential since all trajectories have reached their maximum value and are beginning to decline. Instead, the decline rate becomes more influential in 2200 and 2300 since it plays a crucial role in how quickly

an emissions trajectory approaches zero, and a slow decarbonization rate can increase the cumulative emissions greatly for a given trajectory. This behavior is depicted in Figure 11, which shows that in 2100 (Figure 11a), the emissions growth rate has the second-highest sensitivity index, and in 2200 and 2300 (Figure 11b, c), the decline rate has the second-highest sensitivity index.

Outside of the emissions pathway, Earth system processes have a moderate impact on GMSLR in 2100, but after 2100, they have an extremely small influence since variability in outcomes is dependent on emissions. Since 2100 is closer to present day, cumulative emissions do not have time to vary as much as they do in 2200 or 2300, so the lower variability in emissions dampens the human system influence. The lag in Earth system response also prevents emissions from completely dominating GMSLR in 2100, although the emissions are still the primary contributors to sea level outcomes. Within the Earth system, particular processes have a larger influence on GMSLR outcomes than others. Although components such as the GIS, GSIC, and the carbon cycle have an impact on melting, uncertainty in the climate system and AIS dynamics have a much larger influence on the variability in GMSLR. In 2100, Antarctic annual precipitation, slope of the AIS, and climate sensitivity play the greatest role in the Earth system (Figure 11a). In the climate system, climate sensitivity is important due to its direct role in translating radiative forcing to temperature, which then alters global mean sea level. In the AIS, annual precipitation has a large impact on melting since it affects the surface albedo and the amount of snow accumulation, with a tendency of higher precipitation to counteract melting by increasing albedo and providing stability to the ice sheet. The slope of the AIS also

impacts melting by influencing ice flow dynamics and the stability of the grounding line. A steeper slope can lead to increased ice discharge, grounding-line retreat, and enhanced melting, particularly if AIS fast dynamics are triggered. Combined, these two properties interact to alter AIS melting dynamics. For example, a low annual precipitation combined with a steep slope can reduce stability of the ice sheet, increase the rate of melting, and accelerate grounding-line retreat. The complex dynamics in the AIS interact with other climate processes to determine GMSLR. Climate sensitivity has a large influence on temperature, which then impacts AIS melting via characteristics such as slope and annual precipitation.

Since the influence of the Earth system response is still exceeded by emissions in 2100, it is useful to identify when emissions variability (rather than Earth system uncertainty) becomes the major determining factor of GMSLR variability, as this can be thought of as a proxy for when mitigation begins to manage GMSLR outcomes. To further explore the transition from the influence of Earth system to human system drivers of GMSLR, we plot the GSA results for years nearer to present day: 2070, 2100, 2120, and 2150 (Figure C-3 and Figure C-4). In the year 2070, the Earth system, specifically Antarctica, dominates GMSLR variability. However, by 2100, the influence of emissions dominates since they have more time to alter Earth system processes. This indicates that Earth system dynamics are more influential for GMSLR in the near-term, but between 2070 and 2100, a transition occurs as emissions begin to heavily control climate outcomes.

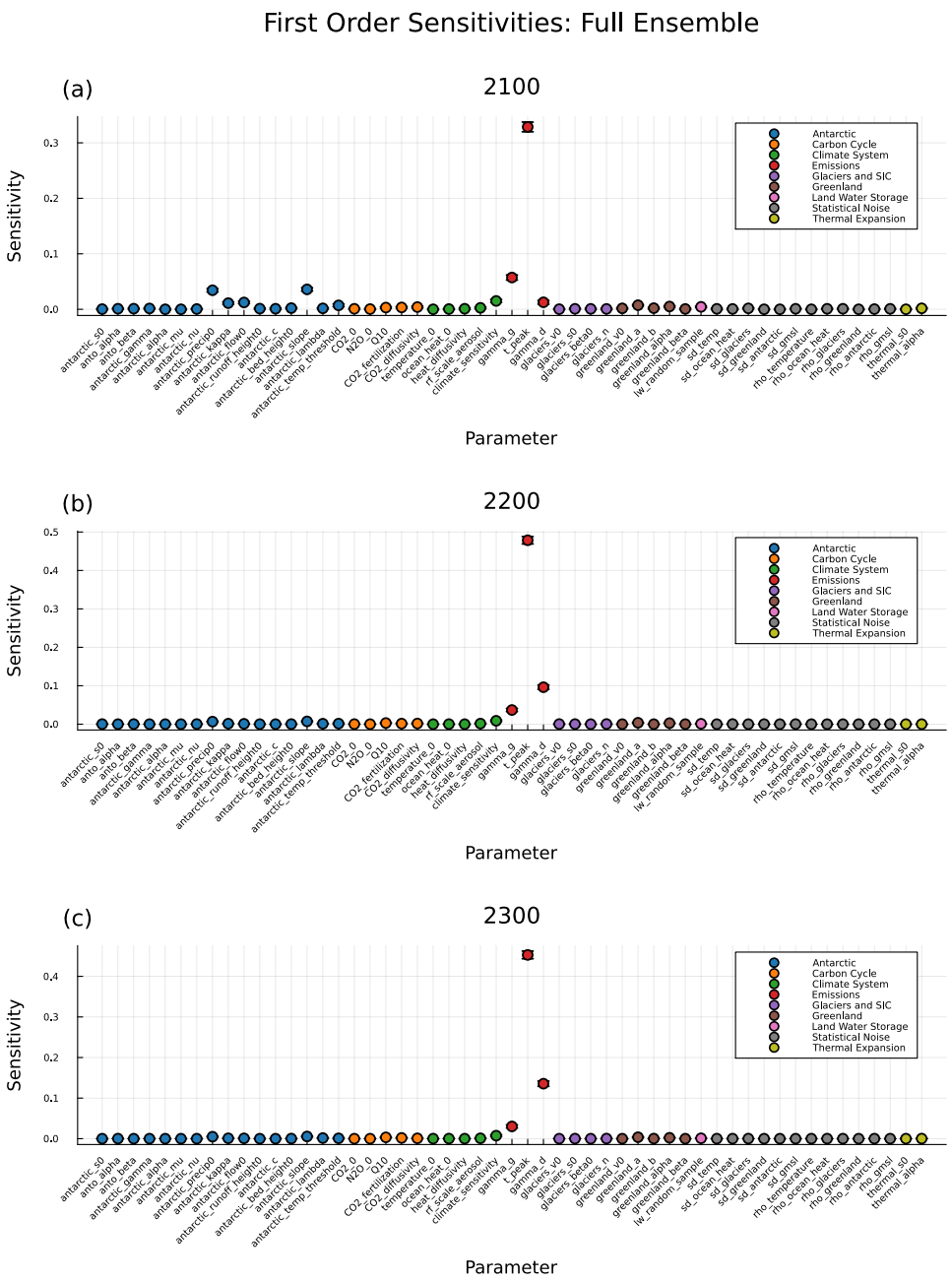

Figure 11. First-order sensitivity indices for the full ensemble of samples on centennial timescales.

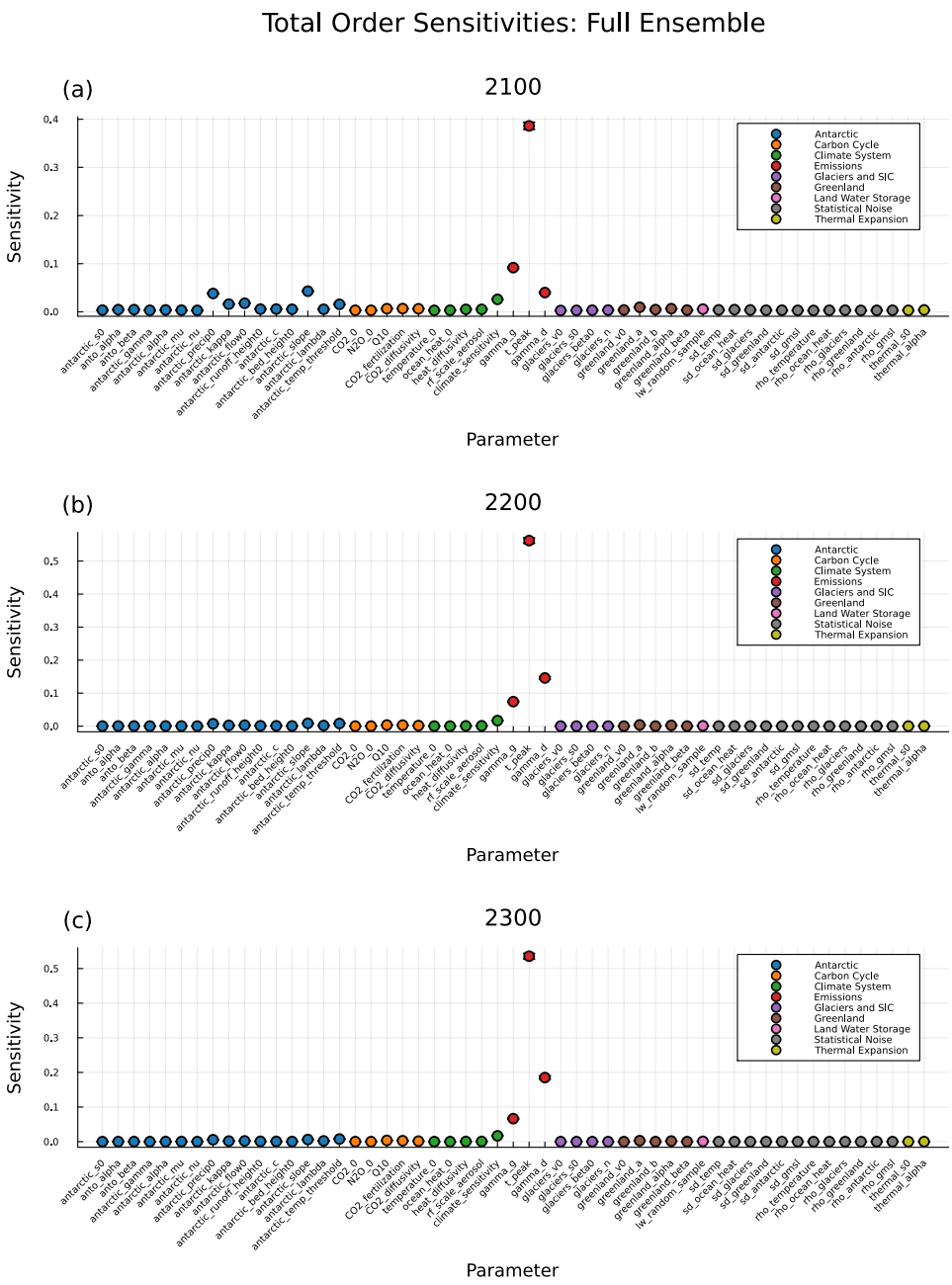

Figure 12. Total-order sensitivity indices for the full ensemble of samples on centennial timescales.

To examine the complete influence of a parameter on GMSLR outcomes, which includes all its interactions with other parameters, we plot the total-order sensitivities in 2100, 2200, and 2300 (Figure 12). Similar to the first-order sensitivities, emissions dominate GMSLR outcomes in all time periods, although Earth system processes play a small role in 2100. Past 2100, the Earth system has very little influence on GMSLR, but out of the Earth system parameters, the Antarctic contribution and climate sensitivity are the most influential in 2200 and 2300. This highlights that the total-order effects of the parameters show the same trends as the first-order effects (Figure 11), which implies that the higher-order interactions of each parameter are relatively small compared to the first-order sensitivities. To visualize the parameter interactions and ensure that this is the case, we create a table of second-order sensitivity indices in 2100, 2200, and 2300 for the full ensemble of samples by selecting the top ten parameter interactions for each of the three years (Table C-1). The indices show that the interaction between growth rate and peaking time is the most influential for all three time periods. Another important interaction is between decline rate and peaking time, and this interaction is approximately equally influential in 2200 and 2300 as that of growth rate and peaking time for those years. However, the interaction between decline rate and peaking time in 2100 has an estimate of zero, which is reasonable given that relatively few emissions trajectories have begun to decline by that time. Out of the second-order interactions, those between different emissions parameters are the most influential, but they still play an overall small role in GMSLR outcomes in all time periods and have a negligible impact on changing the trends seen in the first-order sensitivities.

3.2.2. Grouped GSA

To disaggregate the emissions trajectories into smaller ranges, we conduct a grouped GSA for each of the early, middle, and late peaking groups (see Section 2.1.1 for group criteria). As with the full ensemble, we compute both first- and total-order indices for the parameters to examine their influence on GMSLR outcomes. For the first-order sensitivities, we also develop stacked area plots for each of the three GSA runs, as well as for the full ensemble from the previous section (Figure 13). In principle, first-order indices for all parameters should sum to one for each year. However, since we compute the sensitivity indices using Monte Carlo sampling, the sampling error associated with this approach causes the sum to deviate from one in some years. To improve interpretability of Figure 13, we apply a rescaling using the relative weight of each parameter group so that the sum of the first-order indices is one in all years.

In all four runs, the Earth system processes, specifically Antarctica, dominate first-order sensitivity in the near-term, and the human system (i.e., emissions) dominates in the long-term. In the full ensemble of samples (Figure 13a), emissions almost completely dominate GMSLR outcomes by 2150, explaining about 90% of the variance in the output, and this trend continues out to 2300. This is consistent with the conclusion that Earth system processes dictate outcomes until the climate has sufficient time to respond to sustained emissions, and then the emissions determine GMSLR outcomes.

In the early peaking group (Figure 13b), Earth system processes hold more influence throughout time compared to the full ensemble. The Antarctic, carbon cycle,

and climate system contributions explain around 20% of the output variance in 2150, compared to only 10% for the full ensemble. In the late peaking group (Figure 13d), the Earth system holds about the same influence as in the early group. The more sustained influence of the Earth system in the early and late groups is likely attributed to the particularly low (for early peaking) and high (for late peaking) cumulative emissions that are produced in the two groups. With low emissions, there is a lower probability of high GMSLR, but Earth system parameters with extreme values become particularly influential on GMSLR as a result. With high emissions, there is a higher probability of high GMSLR, but the Earth system heavily dictates the extent of the GMSLR. Although the early and late groups have approximately equal contributions from the Earth system, different contributors within the Earth system hold more importance depending on the peaking group. In the late group, the climate system and the GIS explain more output variance than for early peaking, but Antarctica holds less influence than in the early group. Specifically, the Greenland contribution explains about 10% of the variance in GMSLR output through all years in the late peaking group, which is substantially more than for all the other groups. This is due to the proportional response of GIS melting to temperature increases, which are larger in the late group than the early group. However, Antarctica is less influential in the late group due to the increased likelihood of substantial melting of the AIS (due to high cumulative emissions) regardless of the Antarctic parameters in a certain SOW. In the early group, there are fewer SOWs where substantial melting of the AIS occurs, so the Antarctic processes that alter melting dynamics become more influential on the AIS contribution to GMSLR. Furthermore, the climate system is more sensitive in the late

group compared to the early group, with one of the most influential parameters in the climate system being climate sensitivity. With higher cumulative emissions in the late peaking group, the climate sensitivity becomes more important in determining temperature outcomes, which then impacts sea levels. In the middle peaking group (Figure 13c), emissions more heavily dominate the output variance than for the early and late groups. This is a result of the wider range of cumulative emissions in the middle peaking group, which leads to more variability in climate outcomes and therefore a higher influence of emissions on GMSLR.

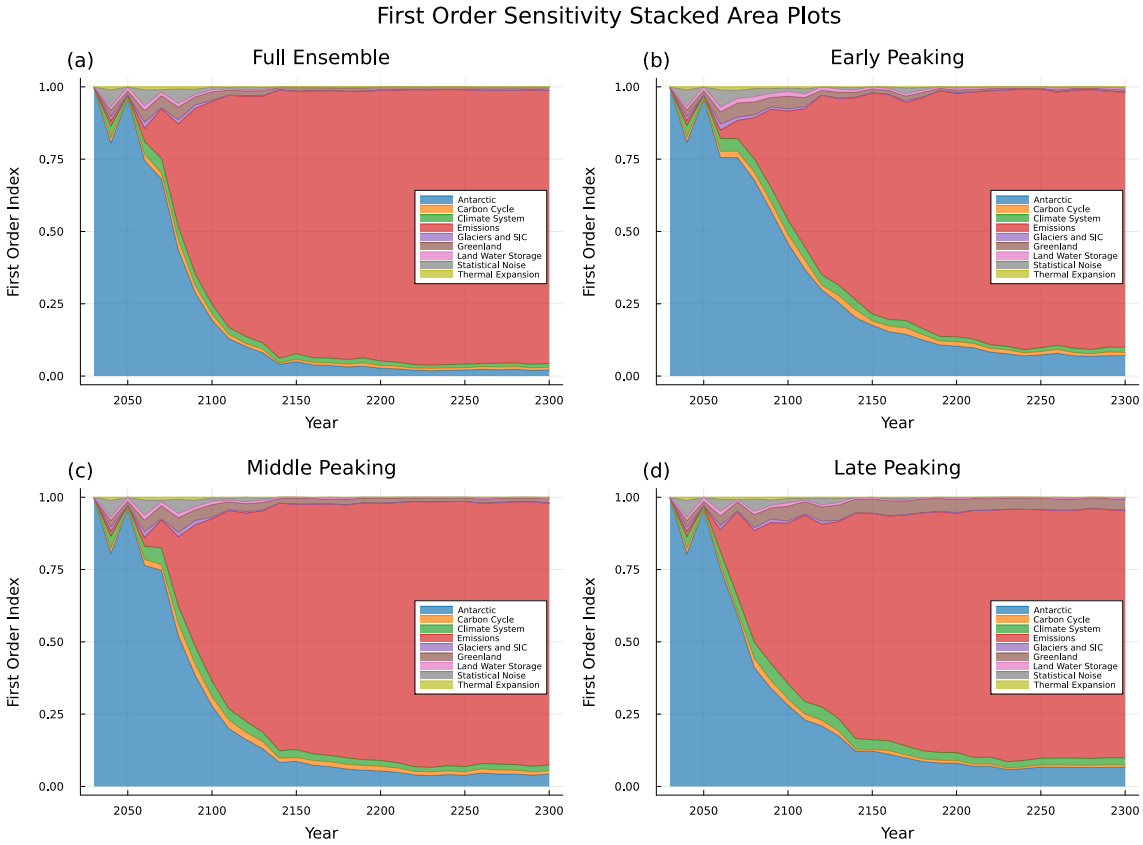

Figure 13. Contribution of parameter groups to first-order sensitivity indices for each GSA run. A rescaling has been applied so that the sum of the indices is one.

In addition to the contributions of parameter groups to first-order sensitivities, the total-order indices are also important for a comprehensive understanding of parameter influences. As with the full ensemble of samples, the second-order interactions are small for all grouped GSA runs and have a negligible influence on the patterns in the total-order sensitivities. Because of this, the first- and total-order sensitivities show nearly identical trends (as with the full ensemble), so we present only the total-order sensitivities here. Since emissions control GMSLR outcomes past 2100 (see Section 3.2.1), we show decadal timescales instead of centennial timescales for the grouped runs. We therefore use the years 2070, 2100, 2120, and 2150 to illustrate the transition of when mitigation begins to manage GMSLR outcomes. The total-order sensitivity indices for the early, middle, and late peaking groups are depicted in Figure 14, Figure 15, and Figure 16, respectively.

For the early and middle peaking groups, Earth system processes dominate GMSLR outcomes in 2070, but this is not the case for the late peaking group. By 2070, the late peaking group is already controlled by emissions, which is reasonable due to the high cumulative emissions produced very quickly in this group. Specifically, the growth rate is the most influential emissions parameter in the late group through all time periods. This is due to the late peaking time for the emissions trajectories in this group, which are not able to peak until at least 2100. Since the trajectories in this group continue to grow for such an extended period of time, the rate at which they grow has the largest impact on warming outcomes. For the early group, all emissions trajectories have peaked before 2050, which is prior to the first year shown in Figure 14. As a result, all emissions trajectories have been declining for a

considerable amount of time, so the rate at which a trajectory decarbonizes becomes the most important factor. Peaking time is important to an extent since it determines the maximum value of emissions reached, but in the longer-term the decarbonization rate heavily dictates the cumulative emissions produced. This behavior is illustrated in Figure 14, where the decline rate and peaking time are the most influential emissions parameters, but the decline rate becomes more influential and peaking time becomes less influential throughout the time period shown. For the middle group (Figure 15), peaking time is the most influential emissions parameter from 2100 onward. This is consistent with the wider range of emissions trajectories in the middle peaking group, resulting in peaking time being the primary factor that determines the quantity of cumulative emissions produced. Following peaking time, growth rate is the most influential in emissions outcomes in the near-term before most trajectories have peaked, but in the longer-term, decline rate becomes more important in determining cumulative emissions. This is depicted in 2100 and 2120 for the middle group, where growth rate is the second-most influential emissions parameter, followed by decline. However, this reverses in 2150, with decline rate surpassing growth rate as the second-most influential emissions parameter.

Outside of the human system, the Earth system plays a key role in the near-term for the early and middle peaking groups. Although Earth system processes are less influential in all time periods for the late peaking group, all three groups show a similar pattern of Earth system parameters that tend to dominate GMSLR outcomes. In all groups and time periods, the Antarctic contribution primarily controls outcomes. Specifically, the Antarctic slope, annual precipitation, proportionality constant for ice

flow, and coefficient for dependency of precipitation on Antarctic temperature are consistently key parameters. The temperature threshold that determines the Antarctic tipping point is also moderately influential. This highlights the complex representation of the AIS in BRICK, since the uncertainties in key relationships and melting dynamics interact to heavily influence outcomes. Following the Antarctic contribution, the climate system and Greenland play an important role as well. Within the Greenland contribution, the parameter that dictates sensitivity of the equilibrium volume of the GIS to changes in temperature is the most influential. This parameter determines the GIS melting in response to warming (see Figure 8), so it is understandable that it would dominate the Greenland contribution. Within the climate system, climate sensitivity is the most influential, followed by a smaller influence from the aerosol scaling factor. The relatively small importance of the climate sensitivity and aerosol scaling factor compared to the Antarctic contribution is inconsistent with the work of Hough & Wong (2022), which finds that those two parameters are consistently the most influential in both low and high radiative forcing groups. Specifically, Hough & Wong (2022) determines that under RCP2.6 in 2100, climate sensitivity is the most important parameter, followed by Antarctic temperature threshold and then aerosol scaling factor. Under RCP8.5, the study identifies the Greenland parameters as the most important contributors, followed by climate sensitivity, aerosol scaling factor, and finally Antarctic Ice Sheet parameters (Hough & Wong, 2022). Within the AIS parameters, Hough & Wong (2022) also finds that the rate of Antarctic fast dynamics has moderate influence, which we do not see here. Instead, we find that the Antarctic contribution is consistently the most important

Earth system group for all peaking times, with the two dominating parameters being Antarctic slope and annual precipitation. This discrepancy could be a result of the deterministic emissions trajectories used in their analysis, whereas here we develop parametrized trajectories with additional degrees of freedom. Due to the disaggregation of emissions parameters that we use, emissions tend to heavily dominate sensitivities past 2100, which could possibly conceal the influence of certain Earth system parameters. We also use a longer timescale that goes out to 2300, which could potentially mask some of the sensitivities seen in their work. Overall, we find that in the near-term, the Earth system controls GMSLR outcomes, but from 2070 to 2100, a transition occurs as emissions begin to completely dominate.

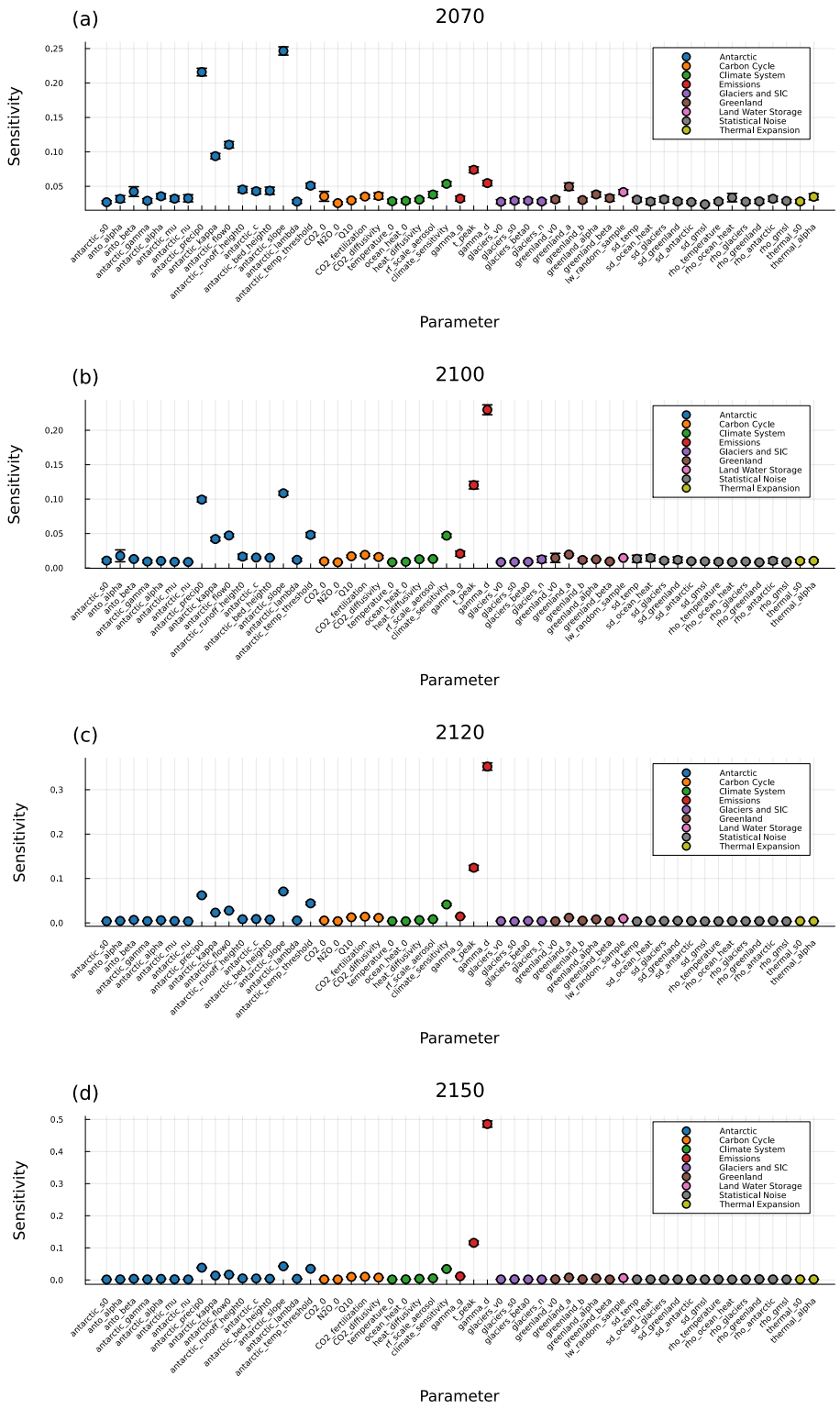

Figure 14. Total-order sensitivity indices for early peaking samples on decadal timescales.

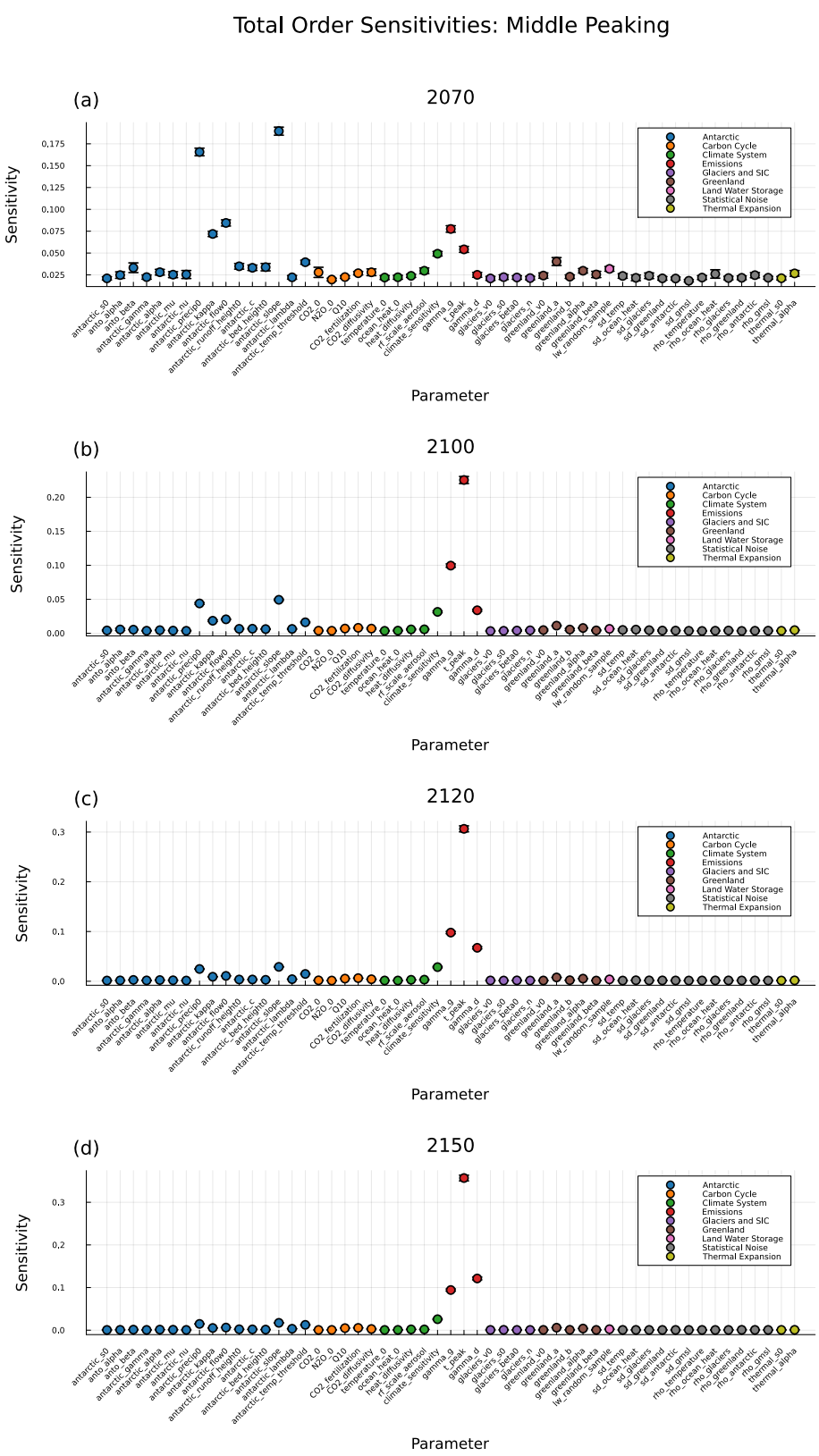

Figure 15. Total-order sensitivity indices for middle peaking samples on decadal timescales.

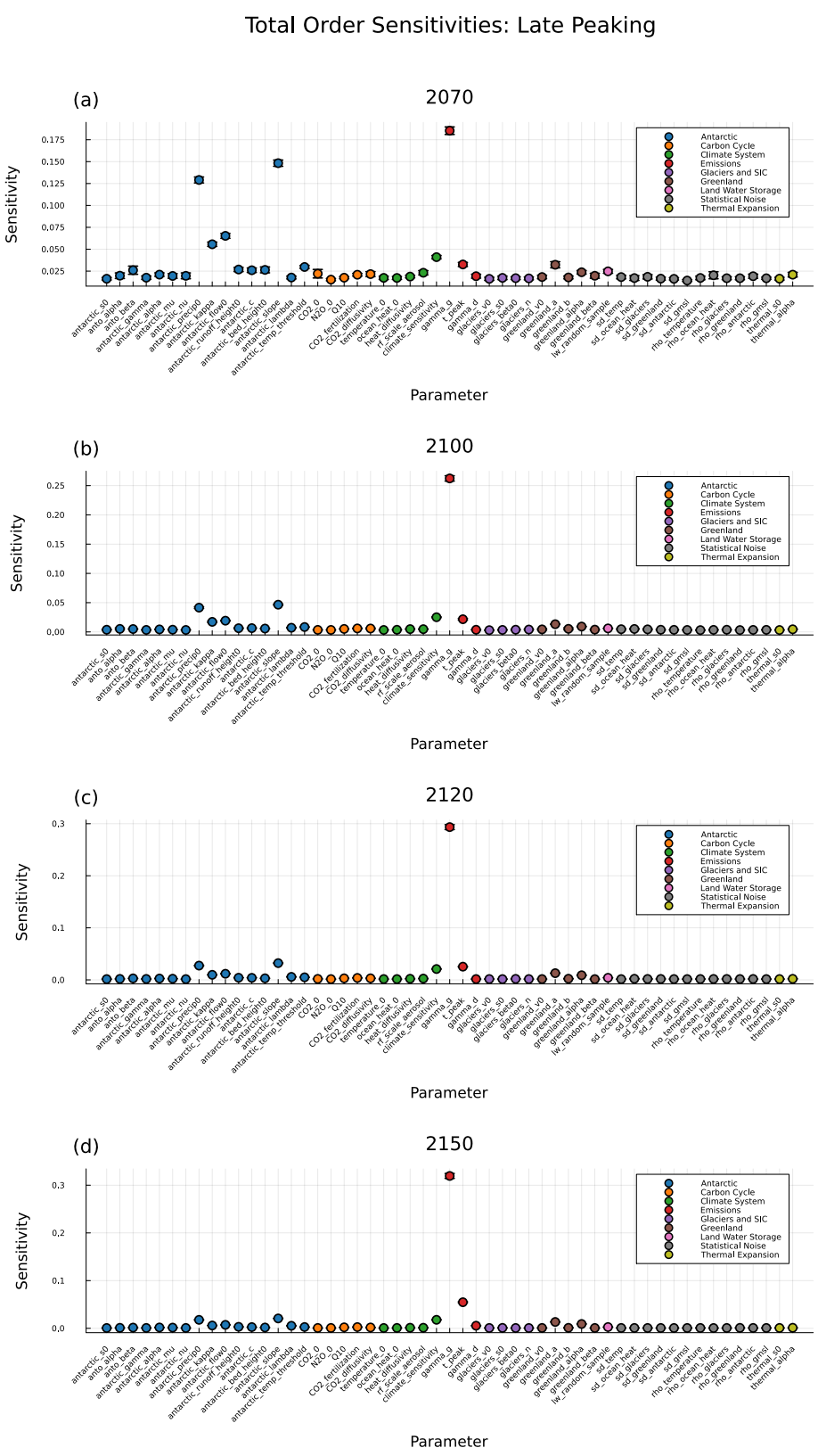

Figure 16. Total-order sensitivity indices for late peaking samples on decadal timescales.

4. DISCUSSION AND CONCLUSIONS

4.1. Caveats and Future Work

In this analysis, we examined how uncertainties in the human system and the Earth system interact to determine climate impacts. We selected SNEASY-BRICK since its short run time made a global sensitivity analysis computationally feasible, which enabled us to determine the drivers of variability in GMSLR over time. However, this modeling framework introduced caveats that are important to mention. One caveat is the representation of ice sheet melting in BRICK. Both the Antarctic and Greenland Ice Sheets are subject to tipping points that lead to rapid mass loss, and there is evidence that Greenland may be approaching a critical threshold that would substantially impact its melting (Boers & Rypdal, 2021). However, this behavior for the GIS is not represented in BRICK. Although BRICK employs a variety of Antarctic system parameters to capture its threshold behavior and potential for fast disintegration, these melting dynamics are not represented for Greenland. Instead, the GIS has a simplistic representation in BRICK where it responds approximately linearly to temperature, which may underestimate its potential for rapid melting after crossing a tipping point. As a result, it is important for future studies to consider whether the simplistic representation of melting dynamics in the GIS is an accurate approximation for real-world outcomes.

Another important caveat is that we did not allow emissions to decline below zero in our representation of emissions pathways. Since the potential role of negative emissions technologies is deeply uncertain (Srikrishnan, Guan, et al., 2022), we made this choice to avoid unrealistic representations of negative emissions in the ensemble

of trajectories. However, this structure neglects potentially substantial emissions reductions that may result from negative emissions technologies, which may lead to an overestimation of climate impacts with our framework. A possible extension of this study would be to include a representation of negative emissions by allowing emissions trajectories to decline below zero, which would provide insight into how negative emissions may impact future climate outcomes.

To expand on the results of this study, one next step is to group different emissions pathways by cumulative emissions in addition to peaking time. Our results highlight that an individual peaking group can lead to a wide range of cumulative emissions and GMSLR outcomes. Grouping by peaking time is useful to examine the timing of climate impacts triggered by threshold behavior, such as ice-sheet instability. However, global radiative forcing, temperature, and GMSLR are instead a result of total cumulative emissions and are less dependent on the exact timescales on which emissions increase and decrease. Because of this, it would be useful to group emissions by both peaking time and cumulative emissions to explore both the temporal dynamics of emissions as well as the total impact of CO_2 released into the atmosphere. Another opportunity for further analysis is the use of scenario discovery, which is an approach that identifies regions of the parameter space that are connected to outcomes of interest (Srikrishnan, Lafferty, et al., 2022). In this case, scenario discovery could be used to identify samples that result in particularly low or high outcomes of GMSLR. Once the samples are identified, they can then be analyzed for trends in human or Earth system parameters to see if any common patterns emerge. Further analysis in these avenues will provide insight into the Earth system response to

uncertain emissions trajectories, which will help improve understanding and management of climate impacts.

4.2. Conclusions

Uncertainties in both the human system and the Earth system compound over time to create highly uncertain outcomes and climate risks. This leads to a wider range of potential climate impacts over time, one of which is global mean sea level rise. Previous studies have primarily explored the interactions between uncertain emissions pathways and the uncertain Earth system response using deterministic, pre-defined emissions scenarios. Here, we develop an ensemble of emissions trajectories using parameters for growth rate, peaking time, and decarbonization rate to examine three key questions: (1) To what extent do different emissions pathways alleviate future climate impacts?, (2) What are the most influential drivers of variability in global mean sea level rise?, and (3) To what extent do these drivers vary over time? We find that as emissions trajectories approach zero, GHG concentrations in the atmosphere begin to stabilize and therefore lead to stable radiative forcing and temperature outcomes. Even after GHG concentrations stabilize, however, there are continued changes in ocean temperatures due to circulation and mixing (Meehl et al., 2012). Because of this, the ocean temperature responds to atmospheric forcing on a longer timescale than the air temperature, leading to higher commitment to GMSLR. Trajectories with early peaking of emissions constrain future GMSLR outcomes, and these pathways rely less on favorable Earth system dynamics to limit GMSLR to a moderate level. However, even under an early peaking group, outcomes for GMSLR

are still sufficiently high to pose substantial climate risks and necessitate adaptation. Rapid mitigation is thus inadequate to fully manage the risks posed by GMSLR, although it does ameliorate the long-term risks. Since the timescale for stabilizing GMSLR is on the lines of centuries, mitigation in the near-term affords additional time for adaptation measures to be implemented for previously committed GMSLR (Meehl et al., 2012).

When considering different emissions trajectories and GMSLR outcomes, we find that the Antarctic and Greenland contributions dominate sea level outcomes in most scenarios. This is consistent with the conclusion of Hough & Wong (2022), which finds that mass loss from the AIS and the GIS drive the long-term risks associated with GMSLR. Of the contributors to GMSLR, both the Antarctic and Greenland Ice Sheets also have the most uncertain outcomes over time. Greenland primarily melts in response to increasing temperatures, whereas Antarctica experiences rapid melting in some states-of-the-world due to thresholds triggering fast melting dynamics. Using a Sobol' sensitivity analysis, we find that the Earth system dominates GMSLR outcomes in the near-term (until around 2070). Specifically, the Antarctic contribution is the most influential Earth system group in determining GMSLR outcomes. Between 2070 and 2100, emissions transition to become the most influential factors, and past 2100, emissions heavily control GMSLR outcomes. However, when trajectories have a late peaking time, emissions begin to control outcomes sooner compared to the early and middle peaking groups.

The results in this analysis exceed the IPCC projections for sea level rise by 2100 and 2150 for all peaking groups. For example, the IPCC estimates that by 2100,

GMSLR will reach 0.63-1.01 meters under the very high GHG emissions scenario (SSP5-8.5) (IPCC, 2021). Under the same scenario, they further estimate that by 2150, GMSLR will reach 0.98-1.88 meters. The IPCC projection is associated with a best estimate of 4.4°C average warming from 2081-2100 (IPCC, 2021), which corresponds to the 94th percentile in 2100 for the late peaking group we consider. We find that the 0.63-1.01 meter GMSLR range in 2100 corresponds to the 4th and 39th percentiles of the late peaking group, and the 0.98-1.88 meter range in 2150 corresponds to the 0.5th and 19th percentiles. All these GMSLR percentiles are below the median, and they fall lower as time progresses from 2100 to 2150. Since the IPCC estimate has a high percentile for global temperature in the late peaking group that results in much lower percentiles for GMSLR, this indicates that the IPCC produces conservative estimates for GMSLR. Specifically for high-warming scenarios, Siegert et al. (2020) describes that it is more likely that we exceed the IPCC range than fall below it, and the estimate of the IPCC is focused at the low end of outcomes. This is also consistent with Garner et al. (2018), which finds that GMSLR estimates from the IPCC are consistently lower than upper estimates from other studies, and the IPCC intentionally provides cautious and conservative estimates of GMSLR. This is partially due to the wide array of stakeholders that the IPCC report targets, and each of these stakeholders have different risk tolerances (Kopp et al., 2023). Furthermore, the IPCC estimate described above is expressed as a “likely” range, which means that the projection has a 66-100% probability of being correct (Siegert et al., 2020). On the reverse end, this also implies there is a 1 in 3 chance that a future outcome will fall outside that range, so there is considerable possibility that the likely range is exceeded. This interpretation can be

lost due to the wide array of stakeholders (many in non-technical domains) that use the IPCC reports, which creates misunderstanding of potential worst-case scenarios (Siegert et al., 2020). To bridge the gap between a conservative estimate and a proper representation of high-end melting scenarios, the IPCC included a low-likelihood, high-impact storyline involving ice-sheet instability caused by MISI and MICI (Kopp et al., 2023). This allows for a better understanding of high-end GMSLR and the processes associated with it while still preserving the widespread utilization of the IPCC reports. Even so, these high-end melting scenarios warrant additional analyses in the IPCC reports to provide more insight into potential drivers and tipping points. Extreme outcomes of GMSLR should not be neglected or seen as impossible scenarios, but it is instead important to better characterize the uncertainties associated with high-end sea level rise to improve resilience to a given outcome.

REFERENCES

Alley, R. B., Anandakrishnan, S., Christianson, K., Horgan, H. J., Muto, A., Parizek, B. R., Pollard, D., & Walker, R. T. (2015). Oceanic Forcing of Ice-Sheet Retreat: West Antarctica and More. *Annual Review of Earth and Planetary Sciences*, *43*(1), 207–231. https://doi.org/10.1146/annurev-earth-060614-105344

Artemieva, I. M. (2022). Antarctica ice sheet basal melting enhanced by high mantle heat. *Earth-Science Reviews*, *226*, 103954. https://doi.org/10.1016/j.earscirev.2022.103954

Bassis, J. N., Berg, B., Crawford, A. J., & Benn, D. I. (2021). Transition to marine ice cliff instability controlled by ice thickness gradients and velocity. *Science*, *372*(6548), 1342–1344. https://doi.org/10.1126/science.abf6271

Boers, N., & Rypdal, M. (2021). Critical slowing down suggests that the western Greenland Ice Sheet is close to a tipping point. *Proceedings of the National Academy of Sciences*, *118*(21), e2024192118. https://doi.org/10.1073/pnas.2024192118

Box, J. E., Hubbard, A., Bahr, D. B., Colgan, W. T., Fettweis, X., Mankoff, K. D., Wehrlé, A., Noël, B., Van Den Broeke, M. R., Wouters, B., Bjørk, A. A., & Fausto, R. S. (2022). Greenland ice sheet climate disequilibrium and committed sea-level rise. *Nature Climate Change*, *12*(9), 808–813. https://doi.org/10.1038/s41558-022-01441-2

Box, J. E., Wehrlé, A., Van As, D., Fausto, R. S., Kjeldsen, K. K., Dachauer, A., Ahlstrøm, A. P., & Picard, G. (2022). Greenland Ice Sheet Rainfall, Heat and Albedo Feedback Impacts From the Mid-August 2021 Atmospheric River. *Geophysical Research Letters*, *49*(11). https://doi.org/10.1029/2021GL097356

Cazenave, A., & Llovel, W. (2010). Contemporary Sea Level Rise. *Annual Review of Marine Science*, *2*(1), 145–173. https://doi.org/10.1146/annurev-marine-120308-081105

Chen, D., Rojas, M., Samset, B. H., Cobb, K., Diongue-Niang, A., Edwards, P., Emori, S., Faria, S. H., Hawkins, E., Hope, P., Huybrechts, P., Meinshausen, M., Mustafa, S. K., Plattner, G.-K., & Tréguier, A. M. (2021). Framing, context,

and methods. In V. Masson-Delmotte, P. Zhai, A. Pirani, S. L. Connors, C. Péan, S. Berger, N. Caud, Y. Chen, L. Goldfarb, M. I. Gomis, M. Huang, K. Leitzell, E. Lonnoy, J. B. R. Matthews, T. K. Maycock, T. Waterfield, Ö. Yelekçi, R. Yu, & B. Zhou (Eds.), *Climate Change 2021: The Physical Science Basis. Contribution of Working Group I to the Sixth Assessment Report of the Intergovernmental Panel on Climate Change* (pp. 147–286). Cambridge University Press. https://doi.org/10.1017/9781009157896.001

Church, J. A., White, N. J., Aarup, T., Wilson, W. S., Woodworth, P. L., Domingues, C. M., Hunter, J. R., & Lambeck, K. (2008). Understanding global sea levels: Past, present and future. *Sustainability Science*, *3*(1), 9–22. https://doi.org/10.1007/s11625-008-0042-4

Davis, P., Nicholls, K., Holland, D., Schmidt, B., Washam, P., Riverman, K., Arthern, R., Vaňková, I., Eayrs, C., Smith, J., Anker, P., Mullen, A., Dichek, D., Lawrence, J., Meister, M., Clyne, E., Basinski-Ferris, A., Rignot, E., Queste, B., & Makinson, K. (2023). Suppressed basal melting in the eastern Thwaites Glacier grounding zone. *Nature*, *614*, 479–485. https://doi.org/10.1038/s41586-022-05586-0

Dixit, V. K., & Rackauckas, C. (2022). GlobalSensitivity.jl: Performant and Parallel GlobalSensitivity Analysis with Julia. *Journal of Open Source Software*, *7*(76), 4561. https://doi.org/10.21105/joss.04561

Fox-Kemper, B., Hewitt, H. T., Xiao, C., Aðalgeirsdóttir, G., Drijfhout, S. S., Edwards, T. L., Golledge, N. R., Hemer, M., Kopp, R. E., Krinner, G., Mix, A., Notz, D., Nowicki, S., Nurhati, I. S., Ruiz, L., Sallée, J.-B., Slangen, A. B. A., & Yu, Y. (2021). Ocean, cryosphere, and sea level change. In V. Masson-Delmotte, P. Zhai, A. Pirani, S. L. Connors, C. Péan, S. Berger, N. Caud, Y. Chen, L. Goldfarb, M. I. Gomis, M. Huang, K. Leitzell, E. Lonnoy, J. B. R. Matthews, T. K. Maycock, T. Waterfield, Ö. Yelekçi, R. Yu, & B. Zhou (Eds.), *Climate Change 2021: The Physical Science Basis. Contribution of Working Group I to the Sixth Assessment Report of the Intergovernmental Panel on Climate Change* (pp. 1211–1362). Cambridge University Press. https://doi.org/10.1017/9781009157896.001

Friedlingstein, P., O'Sullivan, M., Jones, M. W., Andrew, R. M., Gregor, L., Hauck, J., Le Quéré, C., Luijkx, I. T., Olsen, A., Peters, G. P., Peters, W., Pongratz, J., Schwingshackl, C., Sitch, S., Canadell, J. G., Ciais, P., Jackson, R. B., Alin, S. R., Alkama, R., … Zheng, B. (2022). Global Carbon Budget 2022. *Earth System Science Data*, *14*(11), 4811–4900. https://doi.org/10.5194/essd-14-4811-2022

Garner, A. J., Weiss, J. L., Parris, A., Kopp, R. E., Horton, R. M., Overpeck, J. T., & Horton, B. P. (2018). Evolution of 21st Century Sea Level Rise Projections. *Earth's Future*, *6*(11), 1603–1615. https://doi.org/10.1029/2018EF000991

Hansen, J., Russell, G., Lacis, A., Fung, I., Rind, D., & Stone, P. (1985). Climate Response Times: Dependence on Climate Sensitivity and Ocean Mixing. *Science*, *229*(4716), 857–859. https://doi.org/10.1126/science.229.4716.857

Helgeson, C., Srikrishnan, V., Keller, K., & Tuana, N. (2021). Why Simpler Computer Simulation Models Can Be Epistemically Better for Informing Decisions. *Philosophy of Science*, *88*(2), 213–233. https://doi.org/10.1086/711501

Hoegh-Guldberg, O., Jacob, D., Taylor, M., Bindi, M., Brown, S., Camilloni, I., Diedhiou, A., Djalante, R., Ebi, K. L., Engelbrecht, F., Guiot, J., Hijioka, Y., Mehrotra, S., Payne, A., Seneviratne, S. I., Thomas, A., Warren, R., & Zhou, G. (2018). Impacts of 1.5°C Global Warming on Natural and Human Systems. In V. Masson-Delmotte, P. Zhai, H.-O. Pörtner, D. Roberts, J. Skea, P. R. Shukla, A. Pirani, W. Moufouma-Okia, C. Péan, R. Pidcock, S. Connors, J. B. R. Matthews, Y. Chen, X. Zhou, M. I. Gomis, E. Lonnoy, T. Maycock, M. Tignor, & T. Waterfield (Eds.), *Global Warming of 1.5°C. An IPCC Special Report on the impacts of global warming of 1.5°C above pre-industrial levels and related global greenhouse gas emission pathways, in the context of strengthening the global response to the threat of climate change, sustainable development, and efforts to eradicate poverty* (pp. 175–312). Cambridge University Press. https://doi.org/10.1017/9781009157940

Hough, A., & Wong, T. E. (2022). Analysis of the evolution of parametric drivers of high-end sea-level hazards. *Advances in Statistical Climatology, Meteorology and Oceanography*, *8*(1), 117–134. https://doi.org/10.5194/ascmo-8-117-2022

International Institute for Applied Systems Analysis (IIASA). (2009). *RCP Database (version 2.0)* (2.0.5) [dataset]. https://tntcat.iiasa.ac.at/RcpDb/dsd?Action=htmlpage&page=welcome

IPCC. (2021). Summary for policymakers. In V. Masson-Delmotte, P. Zhai, A. Pirani, S. L. Connors, C. Péan, S. Berger, N. Caud, Y. Chen, L. Goldfarb, M. I. Gomis, M. Huang, K. Leitzell, E. Lonnoy, J. B. R. Matthews, T. K. Maycock, T. Waterfield, Ö. Yelekçi, R. Yu, & B. Zhou (Eds.), *Climate Change 2021: The Physical Science Basis. Contribution of Working Group I to the Sixth Assessment Report of the Intergovernmental Panel on Climate Change* (pp. 3–32). Cambridge University Press. https://doi.org/10.1017/9781009157896.001

IPCC. (2022a). Summary for policymakers. In H.-O. Pörtner, D. C. Roberts, M. Tignor, E. S. Poloczanska, K. Mintenbeck, A. Alegría, M. Craig, S. Langsdorf, S. Löschke, V. Möller, A. Okem, & B. Rama (Eds.), *Climate Change 2022: Impacts, Adaptation and Vulnerability. Contribution of Working Group II to the Sixth Assessment Report of the Intergovernmental Panel on Climate Change* (pp. 3–33). Cambridge University Press. https://doi.org/10.1017/9781009325844.001

IPCC. (2022b). Summary for policymakers. In P. R. Shukla, J. Skea, R. Slade, A. A. Khourdajie, R. van Diemen, D. McCollum, M. Pathak, S. Some, P. Vyas, R. Fradera, M. Belkacemi, A. Hasija, G. Lisboa, S. Luz, & J. Malley (Eds.), *Climate Change 2022: Mitigation of Climate Change. Contribution of Working Group III to the Sixth Assessment Report of the Intergovernmental Panel on Climate Change* (pp. 3–48). Cambridge University Press. https://doi.org/10.1017/9781009157926.001

Johnson, G. C., & Lyman, J. M. (2020). Warming trends increasingly dominate global ocean. *Nature Climate Change*, *10*(8), 757–761. https://doi.org/10.1038/s41558-020-0822-0

Joughin, I., Smith, B. E., & Medley, B. (2014). Marine Ice Sheet Collapse Potentially Under Way for the Thwaites Glacier Basin, West Antarctica. *Science*, *344*(6185), 735–738. https://doi.org/10.1126/science.1249055

Keller, K., Helgeson, C., & Srikrishnan, V. (2021). Climate Risk Management. *Annual Review of Earth and Planetary Sciences*, *49*(1), 95–116. https://doi.org/10.1146/annurev-earth-080320-055847

Khan, S. A., Choi, Y., Morlighem, M., Rignot, E., Helm, V., Humbert, A., Mouginot, J., Millan, R., Kjær, K. H., & Bjørk, A. A. (2022). Extensive inland thinning and speed-up of Northeast Greenland Ice Stream. *Nature*, *611*(7937), Article 7937. https://doi.org/10.1038/s41586-022-05301-z

Kopp, R. E., Oppenheimer, M., O'Reilly, J. L., Drijfhout, S. S., Edwards, T. L., Fox-Kemper, B., Garner, G. G., Golledge, N. R., Hermans, T. H. J., Hewitt, H. T., Horton, B. P., Krinner, G., Notz, D., Nowicki, S., Palmer, M. D., Slangen, A. B. A., & Xiao, C. (2023). Communicating future sea-level rise uncertainty and ambiguity to assessment users. *Nature Climate Change*, 1–13. https://doi.org/10.1038/s41558-023-01691-8

Lamontagne, J. R., Reed, P. M., Marangoni, G., Keller, K., & Garner, G. G. (2019). Robust abatement pathways to tolerable climate futures require immediate global action. *Nature Climate Change*, *9*(4), 290–294. https://doi.org/10.1038/s41558-019-0426-8

Lee, J.-Y., Marotzke, J., Bala, G., Cao, L., Corti, S., Dunne, J. P., Engelbrecht, F., Fischer, E., Fyfe, J. C., Jones, C., Maycock, A., Mutemi, J., Ndiaye, O., Panickal, S., & Zhou, T. (2021). Future global climate: Scenario-based projections and near-term information. In V. Masson-Delmotte, P. Zhai, A. Pirani, S. L. Connors, C. Péan, S. Berger, N. Caud, Y. Chen, L. Goldfarb, M. I. Gomis, M. Huang, K. Leitzell, E. Lonnoy, J. B. R. Matthews, T. K. Maycock, T. Waterfield, Ö. Yelekçi, R. Yu, & B. Zhou (Eds.), *Climate Change 2021: The Physical Science Basis. Contribution of Working Group I to the Sixth Assessment Report of the Intergovernmental Panel on Climate Change* (pp. 553–672). Cambridge University Press. https://doi.org/10.1017/9781009157896.001

Lempert, R. J., & Collins, M. T. (2007). Managing the Risk of Uncertain Threshold Responses: Comparison of Robust, Optimum, and Precautionary Approaches. *Risk Analysis*, *27*(4), 1009–1026. https://doi.org/10.1111/j.1539-6924.2007.00940.x

Mahowald, N. M., Ward, D. S., Doney, S. C., Hess, P. G., & Randerson, J. T. (2017). Are the impacts of land use on warming underestimated in climate policy? *Environmental Research Letters*, *12*(9), 094016. https://doi.org/10.1088/1748-9326/aa836d

Martens, P., McEvoy, D., & Chang, C. (2009). The climate change challenge: Linking vulnerability, adaptation, and mitigation. *Current Opinion in Environmental Sustainability*, *1*(1), 14–18. https://doi.org/10.1016/j.cosust.2009.07.010

Martin, T., Biastoch, A., Lohmann, G., Mikolajewicz, U., & Wang, X. (2022). On Timescales and Reversibility of the Ocean's Response to Enhanced Greenland Ice Sheet Melting in Comprehensive Climate Models. *Geophysical Research Letters*, *49*(5). https://doi.org/10.1029/2021GL097114

Meehl, G. A., Hu, A., Tebaldi, C., Arblaster, J. M., Washington, W. M., Teng, H., Sanderson, B. M., Ault, T., Strand, W. G., & White, J. B. (2012). Relative outcomes of climate change mitigation related to global temperature versus sea-level rise. *Nature Climate Change*, *2*(8), Article 8. https://doi.org/10.1038/nclimate1529

Meehl, G. A., Washington, W. M., Collins, W. D., Arblaster, J. M., Hu, A., Buja, L. E., Strand, W. G., & Teng, H. (2005). How Much More Global Warming and Sea Level Rise? *Science*, *307*(5716), 1769–1772. https://doi.org/10.1126/science.1106663

Milne, G. A., Gehrels, W. R., Hughes, C. W., & Tamisiea, M. E. (2009). Identifying the causes of sea-level change. *Nature Geoscience*, *2*(7), 471–478. https://doi.org/10.1038/ngeo544

Morgan, M. G., & Keith, D. W. (2008). Improving the way we think about projecting future energy use and emissions of carbon dioxide. *Climatic Change*, *90*(3), 189–215. https://doi.org/10.1007/s10584-008-9458-1

Morlighem, M., Rignot, E., Binder, T., Blankenship, D., Drews, R., Eagles, G., Eisen, O., Ferraccioli, F., Forsberg, R., Fretwell, P., Goel, V., Greenbaum, J. S., Gudmundsson, H., Guo, J., Helm, V., Hofstede, C., Howat, I., Humbert, A., Jokat, W., … Young, D. A. (2020). Deep glacial troughs and stabilizing ridges unveiled beneath the margins of the Antarctic ice sheet. *Nature Geoscience*, *13*(2), Article 2. https://doi.org/10.1038/s41561-019-0510-8

Morris, J., Reilly, J., Paltsev, S., Sokolov, A., & Cox, K. (2022). Representing Socio-Economic Uncertainty in Human System Models. *Earth's Future*, *10*(4). https://doi.org/10.1029/2021EF002239

Nauels, A., Rogelj, J., Schleussner, C.-F., Meinshausen, M., & Mengel, M. (2017). Linking sea level rise and socioeconomic indicators under the Shared Socioeconomic Pathways. *Environmental Research Letters*, *12*(11), 114002. https://doi.org/10.1088/1748-9326/aa92b6

Oddo, P. C., Lee, B. S., Garner, G. G., Srikrishnan, V., Reed, P. M., Forest, C. E., & Keller, K. (2020). Deep Uncertainties in Sea-Level Rise and Storm Surge Projections: Implications for Coastal Flood Risk Management. *Risk Analysis*, *40*(1), 153–168. https://doi.org/10.1111/risa.12888

O'Hagan, T. (2004). Dicing with the Unknown. *Significance*, *1*(3), 132–133. https://doi.org/10.1111/j.1740-9713.2004.00050.x

O'Neill, B. C., Kriegler, E., Ebi, K. L., Kemp-Benedict, E., Riahi, K., Rothman, D. S., van Ruijven, B. J., van Vuuren, D. P., Birkmann, J., Kok, K., Levy, M., & Solecki, W. (2017). The roads ahead: Narratives for shared socioeconomic

pathways describing world futures in the 21st century. *Global Environmental Change*, *42*, 169–180. https://doi.org/10.1016/j.gloenvcha.2015.01.004

O'Neill, B. C., Kriegler, E., Riahi, K., Ebi, K. L., Hallegatte, S., Carter, T. R., Mathur, R., & van Vuuren, D. P. (2014). A new scenario framework for climate change research: The concept of shared socioeconomic pathways. *Climatic Change*, *122*(3), 387–400. https://doi.org/10.1007/s10584-013-0905-2

Oppenheimer, M., O'Neill, B. C., & Webster, M. (2008). Negative learning. *Climatic Change*, *89*(1–2), 155–172. https://doi.org/10.1007/s10584-008-9405-1

Oreskes, N., Shrader-Frechette, K., & Belitz, K. (1994). Verification, Validation, and Confirmation of Numerical Models in the Earth Sciences. *Science*, *263*(5147), 641–646. https://doi.org/10.1126/science.263.5147.641

Otosaka, I. N., Shepherd, A., Ivins, E. R., Schlegel, N.-J., Amory, C., van den Broeke, M. R., Horwath, M., Joughin, I., King, M. D., Krinner, G., Nowicki, S., Payne, A. J., Rignot, E., Scambos, T., Simon, K. M., Smith, B. E., Sørensen, L. S., Velicogna, I., Whitehouse, P. L., … Wouters, B. (2023). Mass balance of the Greenland and Antarctic ice sheets from 1992 to 2020. *Earth System Science Data*, *15*(4), 1597–1616. https://doi.org/10.5194/essd-15-1597-2023

Pattyn, F., & Morlighem, M. (2020). The uncertain future of the Antarctic Ice Sheet. *Science*, *367*(6484), 1331–1335. https://doi.org/10.1126/science.aaz5487

Pattyn, F., Ritz, C., Hanna, E., Asay-Davis, X., DeConto, R., Durand, G., Favier, L., Fettweis, X., Goelzer, H., Golledge, N. R., Kuipers Munneke, P., Lenaerts, J. T. M., Nowicki, S., Payne, A. J., Robinson, A., Seroussi, H., Trusel, L. D., & Van Den Broeke, M. (2018). The Greenland and Antarctic ice sheets under 1.5 °C global warming. *Nature Climate Change*, *8*(12), 1053–1061. https://doi.org/10.1038/s41558-018-0305-8

Pollard, D., DeConto, R. M., & Alley, R. B. (2015). Potential Antarctic Ice Sheet retreat driven by hydrofracturing and ice cliff failure. *Earth and Planetary Science Letters*, *412*, 112–121. https://doi.org/10.1016/j.epsl.2014.12.035

Reed, P. M., Hadjimichael, A., Malek, K., Karimi, T., Vernon, C. R., Srikrishnan, V., Gupta, R. S., Gold, D. F., Lee, B., Keller, K., Thurber, T. B., & Rice, J. S. (2023). *Addressing Uncertainty in MultiSector Dynamics Research*. Zenodo. https://doi.org/10.5281/zenodo.6110623

Reese, R., Garbe, J., Hill, E. A., Urruty, B., Naughten, K. A., Gagliardini, O., Durand, G., Gillet-Chaulet, F., Chandler, D., Langebroek, P. M., & Winkelmann, R. (2022). The stability of present-day Antarctic grounding lines – Part B: Possible commitment of regional collapse under current climate. *The Cryosphere Discussions*, 1–33. https://doi.org/10.5194/tc-2022-105

Riahi, K., van Vuuren, D. P., Kriegler, E., Edmonds, J., O'Neill, B. C., Fujimori, S., Bauer, N., Calvin, K., Dellink, R., Fricko, O., Lutz, W., Popp, A., Cuaresma, J. C., Kc, S., Leimbach, M., Jiang, L., Kram, T., Rao, S., Emmerling, J., … Tavoni, M. (2017). The Shared Socioeconomic Pathways and their energy, land use, and greenhouse gas emissions implications: An overview. *Global Environmental Change*, *42*, 153–168. https://doi.org/10.1016/j.gloenvcha.2016.05.009

Rignot, E., Velicogna, I., Van Den Broeke, M. R., Monaghan, A., & Lenaerts, J. T. M. (2011). Acceleration of the contribution of the Greenland and Antarctic ice sheets to sea level rise. *Geophysical Research Letters*, *38*(5). https://doi.org/10.1029/2011GL046583

Robinson, A., Calov, R., & Ganopolski, A. (2012). Multistability and critical thresholds of the Greenland ice sheet. *Nature Climate Change*, *2*(6), Article 6. https://doi.org/10.1038/nclimate1449

Rohmer, J., Lincke, D., Hinkel, J., Le Cozannet, G., Lambert, E., & Vafeidis, A. T. (2021). Unravelling the Importance of Uncertainties in Global-Scale Coastal Flood Risk Assessments under Sea Level Rise. *Water*, *13*(6), Article 6. https://doi.org/10.3390/w13060774

Ruckert, K. L., Shaffer, G., Pollard, D., Guan, Y., Wong, T. E., Forest, C. E., & Keller, K. (2017). Assessing the Impact of Retreat Mechanisms in a Simple Antarctic Ice Sheet Model Using Bayesian Calibration. *PLOS ONE*, *12*(1), e0170052. https://doi.org/10.1371/journal.pone.0170052

Ruckert, K. L., Srikrishnan, V., & Keller, K. (2019). Characterizing the deep uncertainties surrounding coastal flood hazard projections: A case study for Norfolk, VA. *Scientific Reports*, *9*(1), Article 1. https://doi.org/10.1038/s41598-019-47587-6

Sadai, S., Condron, A., DeConto, R., & Pollard, D. (2020). Future climate response to Antarctic Ice Sheet melt caused by anthropogenic warming. *Science Advances*, *6*(39), eaaz1169. https://doi.org/10.1126/sciadv.aaz1169

Saltelli, A. (2002). Making best use of model evaluations to compute sensitivity indices. *Computer Physics Communications*, *145*(2), 280–297. https://doi.org/10.1016/S0010-4655(02)00280-1

Saltelli, A., Ratto, M., Andres, T., Campolongo, F., Cariboni, J., Gatelli, D., Saisana, M., & Tarantola, S. (2008). *Global Sensitivity Analysis. The Primer*. John Wiley & Sons, Ltd.

Siegert, M., Alley, R. B., Rignot, E., Englander, J., & Corell, R. (2020). Twenty-first century sea-level rise could exceed IPCC projections for strong-warming futures. *One Earth*, *3*(6), 691–703. https://doi.org/10.1016/j.oneear.2020.11.002

Sobol′, I. M. (2001). Global sensitivity indices for nonlinear mathematical models and their Monte Carlo estimates. *Mathematics and Computers in Simulation*, *55*(1–3), 271–280. https://doi.org/10.1016/S0378-4754(00)00270-6

Srikrishnan, V., Guan, Y., Tol, R. S. J., & Keller, K. (2022). Probabilistic projections of baseline twenty-first century CO2 emissions using a simple calibrated integrated assessment model. *Climatic Change*, *170*(3), 37. https://doi.org/10.1007/s10584-021-03279-7

Srikrishnan, V., Lafferty, D. C., Wong, T. E., Lamontagne, J. R., Quinn, J. D., Sharma, S., Molla, N. J., Herman, J. D., Sriver, R. L., Morris, J. F., & Lee, B. S. (2022). Uncertainty Analysis in Multi-Sector Systems: Considerations for Risk Analysis, Projection, and Planning for Complex Systems. *Earth's Future*, *10*(8). https://doi.org/10.1029/2021EF002644

Stokes, C. R., Abram, N. J., Bentley, M. J., Edwards, T. L., England, M. H., Foppert, A., Jamieson, S. S. R., Jones, R. S., King, M. A., Lenaerts, J. T. M., Medley, B., Miles, B. W. J., Paxman, G. J. G., Ritz, C., Van De Flierdt, T., & Whitehouse, P. L. (2022). Response of the East Antarctic Ice Sheet to past and future climate change. *Nature*, *608*(7922), 275–286. https://doi.org/10.1038/s41586-022-04946-0

Tebaldi, C., Ranasinghe, R., Vousdoukas, M., Rasmussen, D. J., Vega-Westhoff, B., Kirezci, E., Kopp, R. E., Sriver, R., & Mentaschi, L. (2021). Extreme sea levels at different global warming levels. *Nature Climate Change*, *11*(9), 746–751. https://doi.org/10.1038/s41558-021-01127-1

Trusel, L. D., Das, S. B., Osman, M. B., Evans, M. J., Smith, B. E., Fettweis, X., McConnell, J. R., Noël, B. P. Y., & Van Den Broeke, M. R. (2018). Nonlinear rise in Greenland runoff in response to post-industrial Arctic warming. *Nature*, *564*(7734), 104–108. https://doi.org/10.1038/s41586-018-0752-4

Urban, N. M., & Keller, K. (2010). Probabilistic hindcasts and projections of the coupled climate, carbon cycle and Atlantic meridional overturning circulation system: A Bayesian fusion of century-scale observations with a simple model. *Tellus A: Dynamic Meteorology and Oceanography*, *62*(5), 737–750. https://doi.org/10.1111/j.1600-0870.2010.00471.x

Urruty, B., Hill, E. A., Reese, R., Garbe, J., Gagliardini, O., Durand, G., Gillet-Chaulet, F., Gudmundsson, G. H., Winkelmann, R., Chekki, M., Chandler, D., & Langebroek, P. M. (2022). The stability of present-day Antarctic grounding lines – Part A: No indication of marine ice sheet instability in the current geometry. *The Cryosphere Discussions*, 1–34. https://doi.org/10.5194/tc-2022-104

Vega-Westhoff, B., Sriver, R. L., Hartin, C., Wong, T. E., & Keller, K. (2020). The Role of Climate Sensitivity in Upper-Tail Sea Level Rise Projections. *Geophysical Research Letters*, *47*(6). https://doi.org/10.1029/2019GL085792

WCRP Global Sea Level Budget Group. (2018). Global sea-level budget 1993–present. *Earth System Science Data*, *10*(3), 1551–1590. https://doi.org/10.5194/essd-10-1551-2018

Wong, T. E., Bakker, A. M. R., & Keller, K. (2017). Impacts of Antarctic fast dynamics on sea-level projections and coastal flood defense. *Climatic Change*, *144*(2), 347–364. https://doi.org/10.1007/s10584-017-2039-4

Wong, T. E., Bakker, A. M. R., Ruckert, K., Applegate, P., Slangen, A. B. A., & Keller, K. (2017). BRICK v0.2, a simple, accessible, and transparent model framework for climate and regional sea-level projections. *Geoscientific Model Development*, *10*(7), 2741–2760. https://doi.org/10.5194/gmd-10-2741-2017

Wong, T. E., & Keller, K. (2017). Deep Uncertainty Surrounding Coastal Flood Risk Projections: A Case Study for New Orleans. *Earth's Future*, *5*(10), 1015–1026. https://doi.org/10.1002/2017EF000607

Wong, T. E., Rennels, L., Errickson, F., Srikrishnan, V., Bakker, A., Keller, K., & Anthoff, D. (2022a). MimiBRICK.jl: A Julia package for the BRICK model for sea-level change in the Mimi integrated modeling framework. *Journal of Open Source Software*, *7*(76), 4556. https://doi.org/10.21105/joss.04556

Wong, T. E., Rennels, L., Errickson, F., Srikrishnan, V., Bakker, A., Keller, K., & Anthoff, D. (2022b). *Model output supporting MimiBRICK v1.1.0* (1.1.0) [dataset]. https://doi.org/10.5281/zenodo.6626335

Young, T. J., Christoffersen, P., Bougamont, M., Tulaczyk, S. M., Hubbard, B., Mankoff, K. D., Nicholls, K. W., & Stewart, C. L. (2022). Rapid basal melting of the Greenland Ice Sheet from surface meltwater drainage. *Proceedings of the National Academy of Sciences*, *119*(10), e2116036119. https://doi.org/10.1073/pnas.2116036119

Zemp, M., Huss, M., Thibert, E., Eckert, N., McNabb, R., Huber, J., Barandun, M., Machguth, H., Nussbaumer, S. U., Gärtner-Roer, I., Thomson, L., Paul, F., Maussion, F., Kutuzov, S., & Cogley, J. G. (2019). Global glacier mass changes and their contributions to sea-level rise from 1961 to 2016. *Nature*, *568*(7752), 382–386. https://doi.org/10.1038/s41586-019-1071-0

APPENDIX A: RADIATIVE FORCING BEHAVIOR

Past 2200, the radiative forcing in Figure 4b exhibits a change in behavior, where its oscillatory values experience a jump and abruptly flatten out to become constant. This behavior is primarily an artifact of the data in the RCP Database (International Institute for Applied Systems Analysis (IIASA), 2009). Due to the values in the dataset, the input matching method that we use creates sudden transitions in radiative forcing. As described in Section 2.1.1, we match inputs each year for N_2O concentration, aerosol forcing, and other forcing to the RCP scenario that most closely matches the emissions for a trajectory. In the RCP Database, the time series for other forcing is the origin of the oscillating values in the total radiative forcing. The values for other forcing in all RCP scenarios except RCP2.6 abruptly transition from oscillatory forcing to constant values. For RCP4.5 and RCP6.0, this transition occurs in 2150, and for RCP8.5, this transition occurs in 2250. If a trajectory reaches zero emissions, the RCP scenario that most closely matches the emissions will be RCP4.5. Since RCP2.6 assumes negative emissions, it will never be the closest scenario to any trajectory after it becomes negative, as we do not allow the emissions curves to decline below zero. As a result, this oscillatory radiative forcing behavior will not be present after 2250 for any trajectories considered. This approach also creates jumps in forcing, since an emissions trajectory may abruptly transition to matching more closely to a different RCP scenario as it increases or declines toward zero.

APPENDIX B: SNEASY-BRICK CALIBRATION AND GSA

In Bayesian statistics, the "prior" degree of belief about a parameter's uncertainty is modified to reflect new information that has been acquired, which is then updated to the "posterior" uncertainty (O'Hagan, 2004). This is shown in Bayes' theorem:

$$p(\theta|y) = \frac{p(y|\theta)}{p(y)} p(\theta) \quad \text{(A-1)}$$

where $p(\theta|y)$ is the posterior, $p(y|\theta)$ is the likelihood, $p(y)$ is the normalizing constant or marginal likelihood, and $p(\theta)$ is the prior. To visualize how the prior is updated to the posterior, we show the marginal distributions for selected BRICK parameters in Figure B-1. We select the parameters in the Antarctic and Greenland groups since the values defined by their posterior distributions drive the melting dynamics in the AIS and the GIS, which are key contributors to GMSLR. The prior is updated to the posterior via the calibration of SNEASY-BRICK.

Estimating the posterior distribution is a crucial step in model calibration since it represents the updated knowledge of a parameter's behavior based on observed data. For SNEASY-BRICK, this is performed using Markov chain Monte Carlo (MCMC). MCMC is a standard approach for numerically approximating Bayesian posterior distributions, and it does so by constructing a Markov chain to systematically sample from the posterior distribution (Helgeson et al., 2021; Reed et al., 2023). MCMC can require a large number of model evaluations, and for SNEASY-BRICK, the chain is run for 20 million iterations (Wong, Bakker, Ruckert, et al., 2017). For samples in a Markov chain, there is a transient portion prior to convergence to the stationary

distribution, which in the case of MCMC is the posterior distribution. To ensure that the samples represent the posterior distribution, samples in the transient portion are discarded as burn-in. The length of burn-in can be determined by evidence accumulated from a variety of heuristics, such as comparing the kernel density plot after half of the chain to the plot for the full chain. For the parameters in SNEASY-BRICK, 1 million iterations at the beginning of the chain are removed for burn-in. In the remaining iterations, some amount of autocorrelation is present due to the correlation among parameters and the tendency of a chain to remain in a certain region of the parameter space before exploring other regions. Because of this, a representative subset of samples is selected from the remaining 19 million iterations to reduce the impact of autocorrelation while preserving the underlying posterior distribution. This subset contains 10,000 samples, a size that balances the tradeoff between computational efficiency and the statistical precision offered by a larger sample size.

We use this subsample of 10,000 correlated samples for the GSA. When there are correlated parameters in a GSA, it can be difficult to isolate the individual influence of a parameter on the model output. To address this, we increase the parameter independence for the GSA by using kernel density perturbations to nudge parameters from the sampled MCMC chain member. For a given MCMC member, each variable is sampled from a normal distribution centered on the chain and with the bandwidth of the kernel density estimator as the standard deviation. The sampled values are constrained by using the minimum/maximum values of each marginal posterior as the sampling bounds. We sample an additional parameter, the land-water

storage random sample, to examine the impact of uncertainties in land-water storage on GMSLR. The final design matrices for the GSA each contain 10,000 samples of 53 parameters, which includes both the emissions and Earth system parameters. To ensure that the sensitivity indices of each parameter are accurate, we use bootstrapping to compute confidence intervals. We find that 1,000 bootstrap samples produce sensitivity indices with sufficiently small variability, resulting in an unambiguous rank of the parameters' influence on GMSLR.

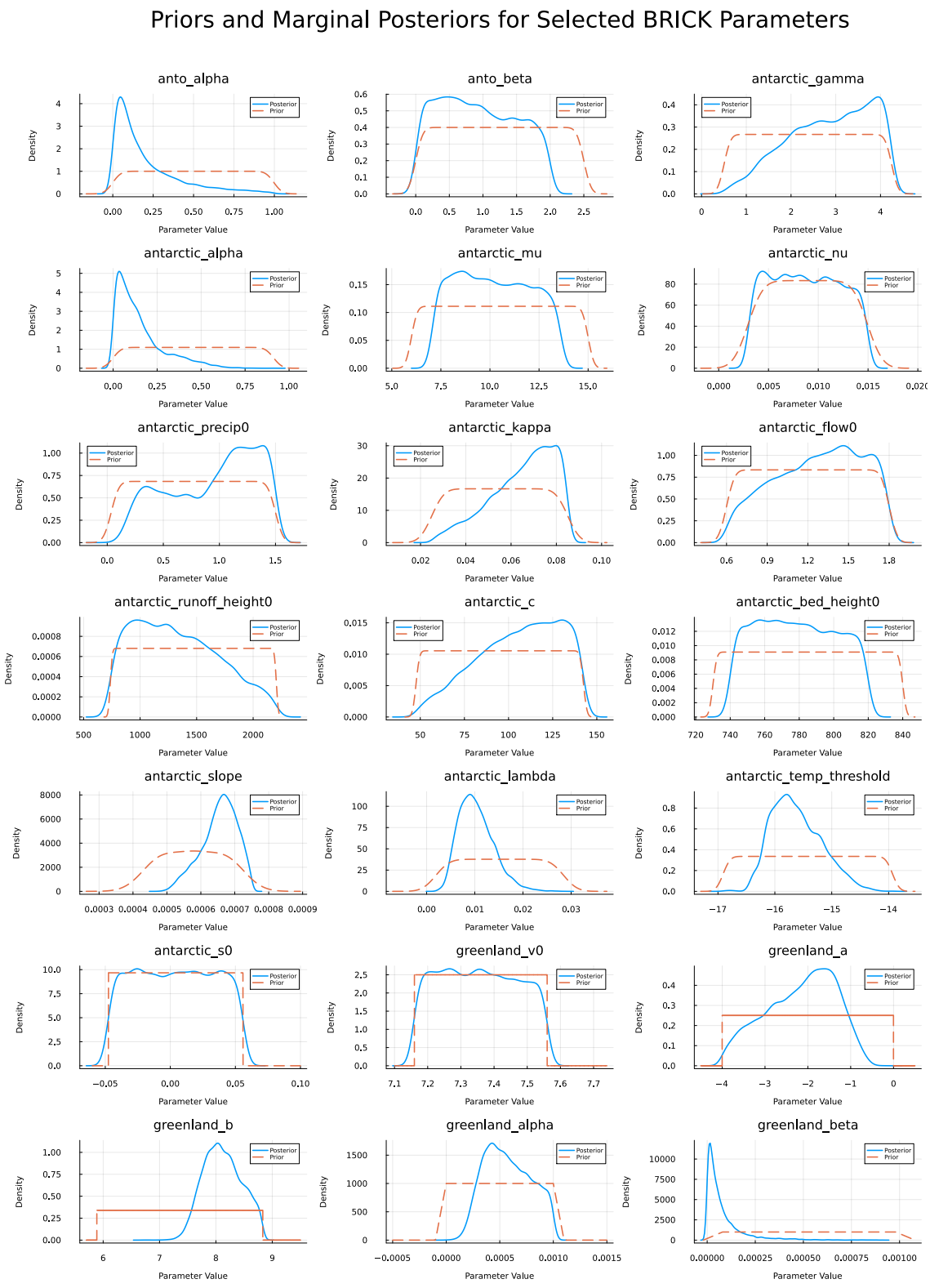

Figure B-1. Marginal distributions for Antarctic and Greenland parameters in BRICK.

APPENDIX C: SUPPLEMENTAL RESULTS

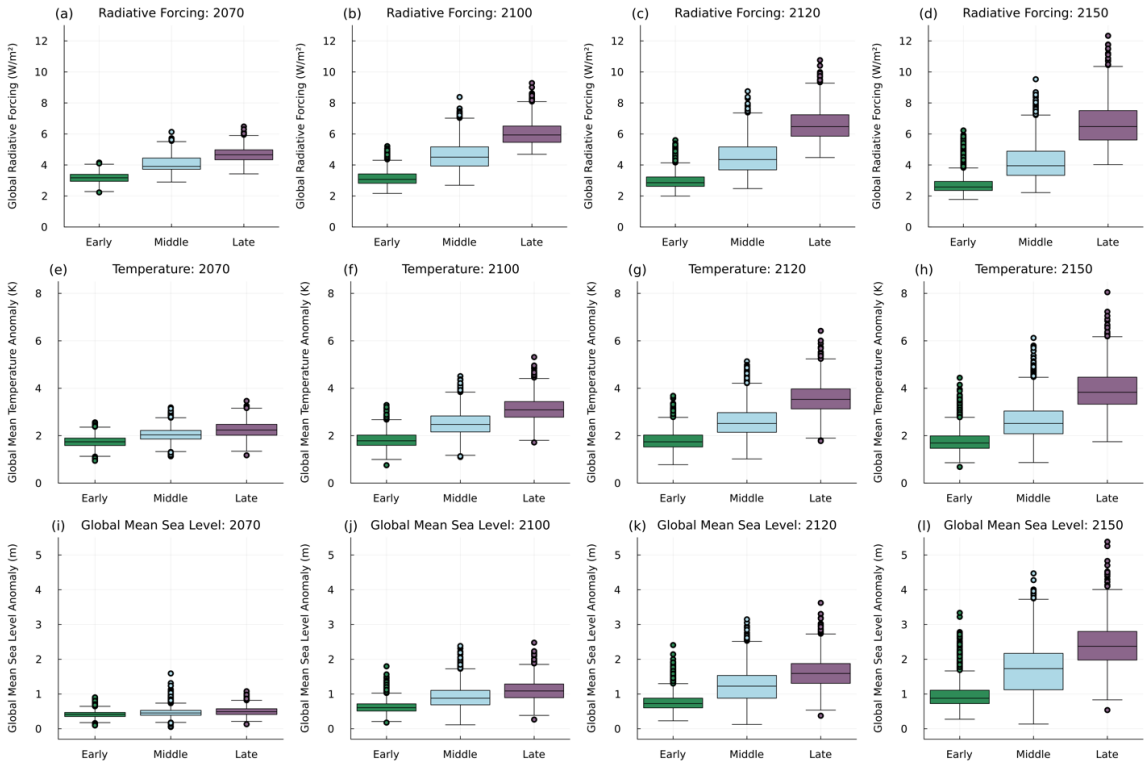

Figure C-1. Radiative forcing, temperature, and GMSLR outcomes across peaking groups and a selection of years near present day (2070, 2100, 2120, and 2150).

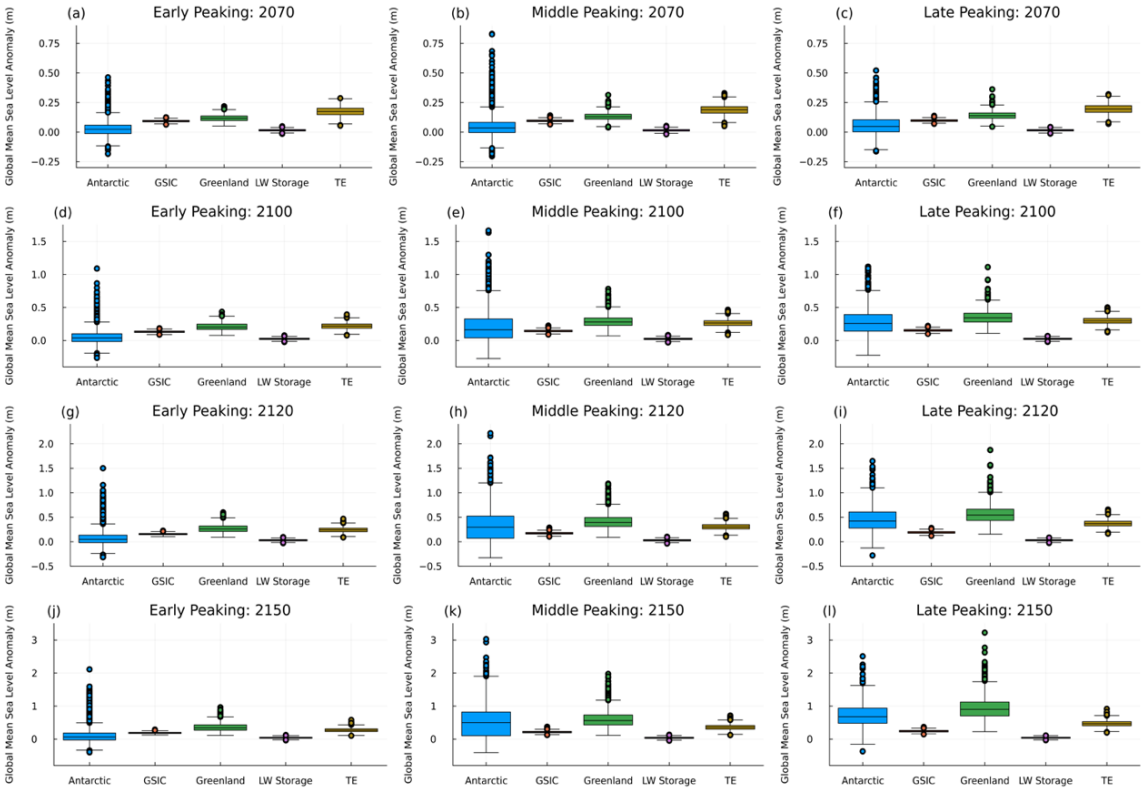

Figure C-2. Contributors to GMSLR across peaking groups and a selection of years near present day (2070, 2100, 2120, and 2150).

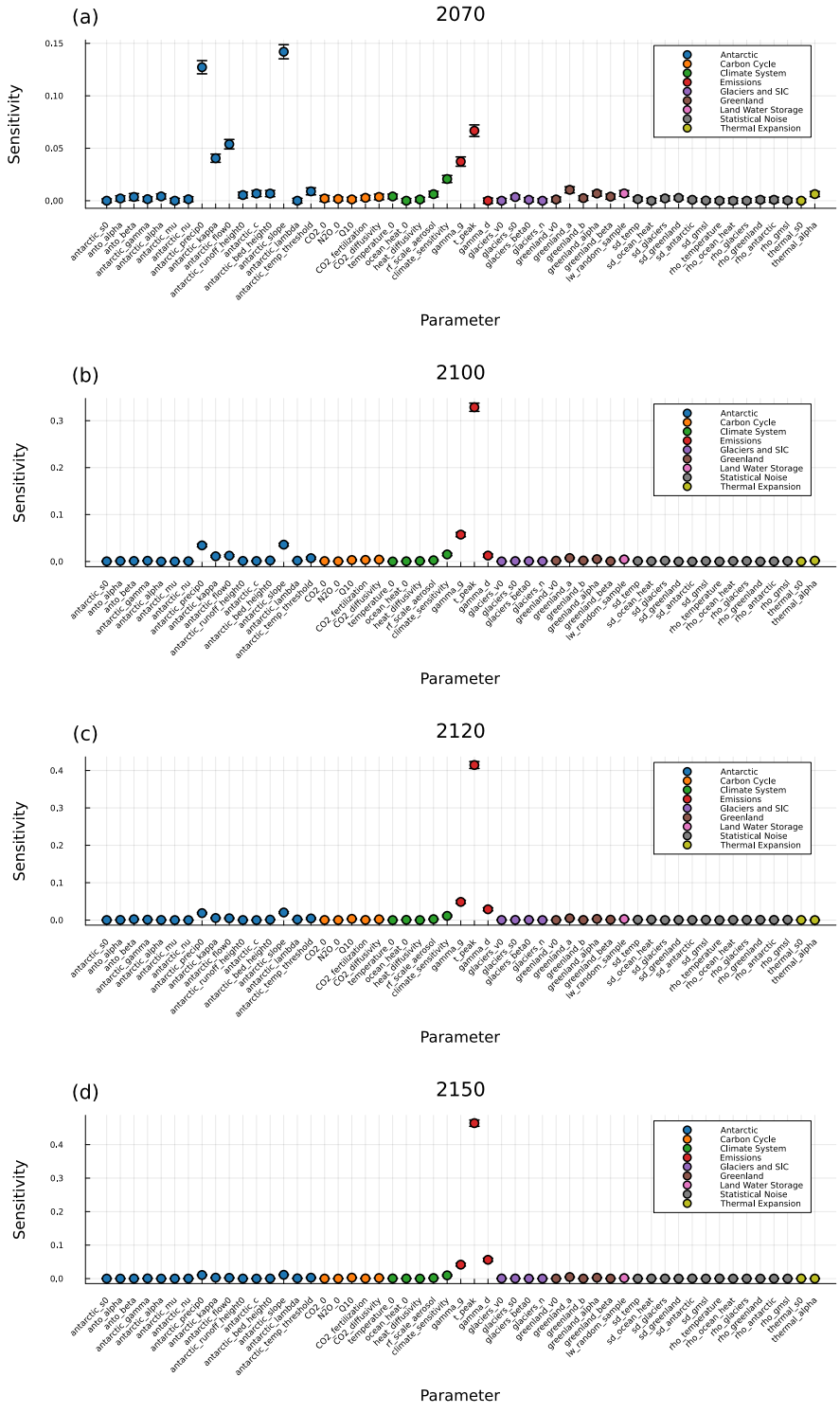

Figure C-3. First-order sensitivity indices for the full ensemble of samples on decadal timescales.

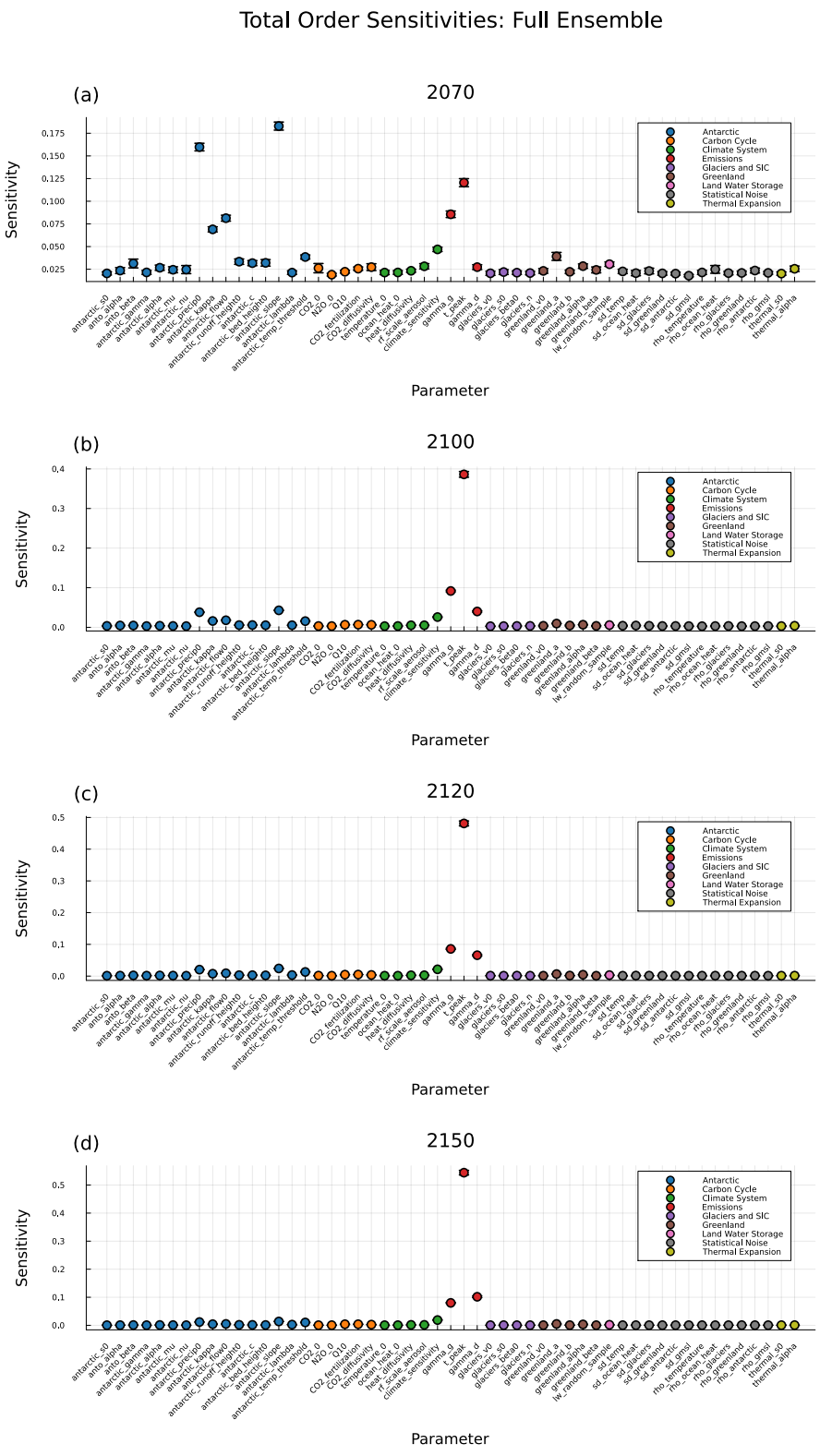

Figure C-4. Total-order sensitivity indices for the full ensemble of samples on decadal timescales.

Table C-1. Second-order sensitivity indices for selected parameter interactions in the full ensemble of samples for the years 2100, 2200, and 2300. Bold values indicate the best estimate for the second-order index of each parameter combination for each year. Boxes shaded green and red indicate the lower and upper bounds, respectively, of the 95% confidence interval.

Parameter 1	Parameter 2	2100		2200		2300	
gamma_g	t_peak	**0.03638**		**0.03818**		**0.03195**	
		0.02804	0.04471	0.03059	0.04576	0.02519	0.03872
t_peak	gamma_d	**0**		**0.03711**		**0.03840**	
		0	0.01123	0.02439	0.04983	0.02570	0.05110
gamma_d	sd_glaciers	**0.00714**		**0.01018**		**0.00892**	
		0.00241	0.01188	0.00243	0.01792	0	0.01792
gamma_d	rho_ocean_heat	**0.00715**		**0.01006**		**0.00889**	
		0.00242	0.01187	0.00232	0.01781	0	0.01789
gamma_d	rho_gmsl	**0.00715**		**0.00999**		**0.00897**	
		0.00241	0.01189	0.00224	0.01774	0	0.01797
gamma_d	greenland_v0	**0.00726**		**0.01012**		**0.00894**	
		0.00253	0.01199	0.00238	0.01787	0	0.01794
gamma_d	Q10	**0.00720**		**0.01013**		**0.00923**	
		0.00247	0.01194	0.00236	0.01789	0.00022	0.01823
gamma_d	CO2_fertilization	**0.00715**		**0.01011**		**0.00891**	
		0.00237	0.01194	0.00236	0.01787	0	0.01791
gamma_d	CO2_diffusivity	**0.00668**		**0.00998**		**0.00914**	
		0.00193	0.01142	0.00223	0.01773	0.00015	0.01813
gamma_d	anto_alpha	**0.00714**		**0.01001**		**0.00892**	
		0.00241	0.01187	0.00226	0.01776	0	0.01793
gamma_d	anto_beta	**0.00718**		**0.01007**		**0.00909**	
		0.00244	0.01193	0.00232	0.01783	0.00008	0.01809
gamma_d	antarctic_c	**0.00728**		**0.01030**		**0.00920**	
		0.00252	0.01204	0.00256	0.01803	0.00021	0.01819
gamma_d	antarctic_mu	**0.00698**		**0.01021**		**0.00905**	
		0.00227	0.01170	0.00247	0.01795	0.00005	0.01804
gamma_d	antarctic_precip0	**0.00681**		**0.01034**		**0.00916**	
		0.00206	0.01157	0.00257	0.01810	0.00014	0.01818
gamma_d	antarctic_runoff_height0	**0.00689**		**0.01018**		**0.00897**	
		0.00217	0.01161	0.00246	0.01790	0.00000	0.01794
gamma_d	antarctic_bed_height0	**0.00688**		**0.01031**		**0.00917**	
		0.00214	0.01161	0.00256	0.01807	0.00016	0.01818
gamma_d	antarctic_lambda	**0.00688**		**0.01061**		**0.00966**	
		0.00216	0.01160	0.00285	0.01837	0.00065	0.01867
gamma_d	antarctic_alpha	**0.00691**		**0.01011**		**0.00912**	
		0.00217	0.01166	0.00236	0.01787	0.00011	0.01813
gamma_d	lw_random_sample	**0.00696**		**0.01029**		**0.00917**	
		0.00223	0.01169	0.00255	0.01803	0.00017	0.01817

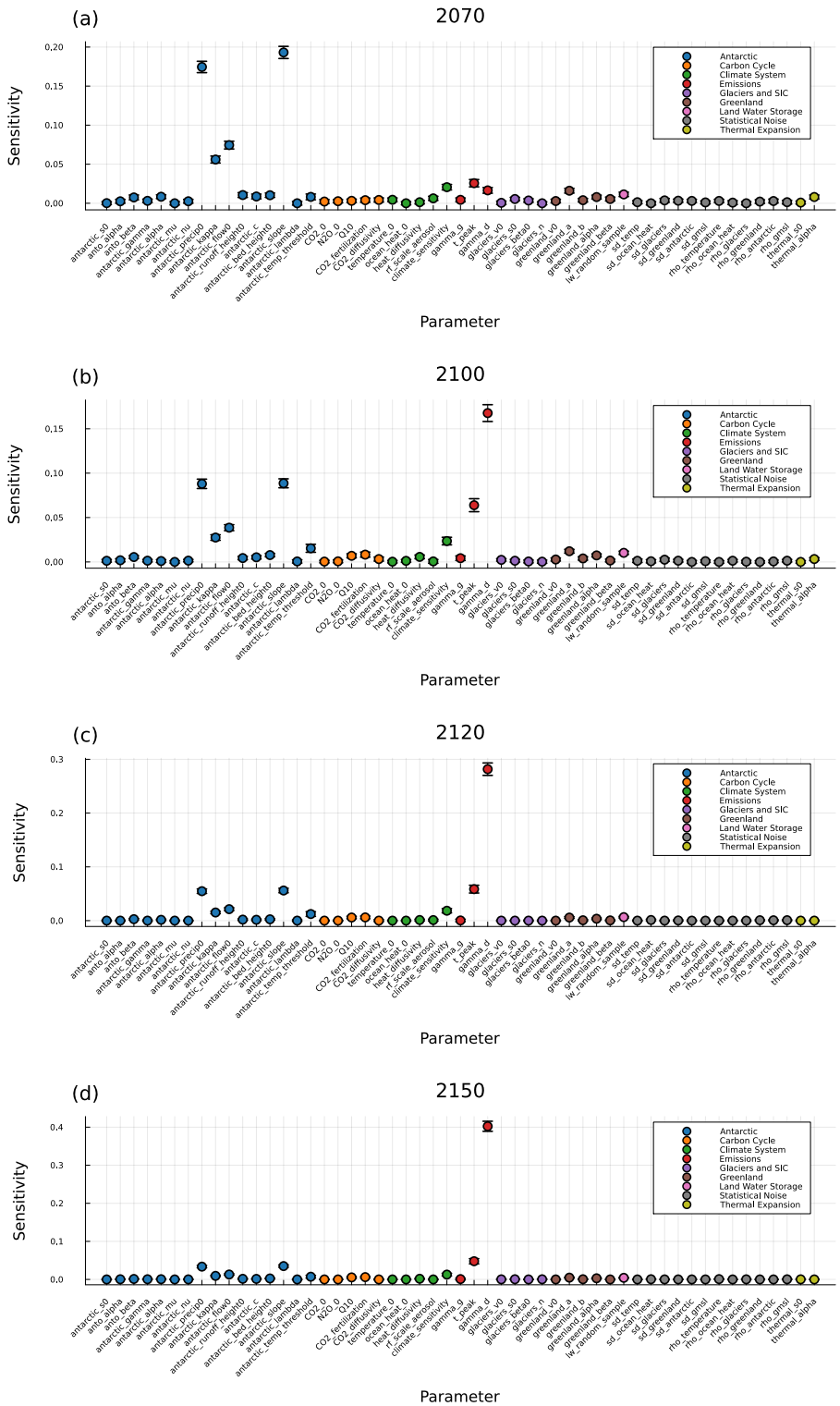

Figure C-5. First-order sensitivity indices for early peaking samples on decadal timescales.

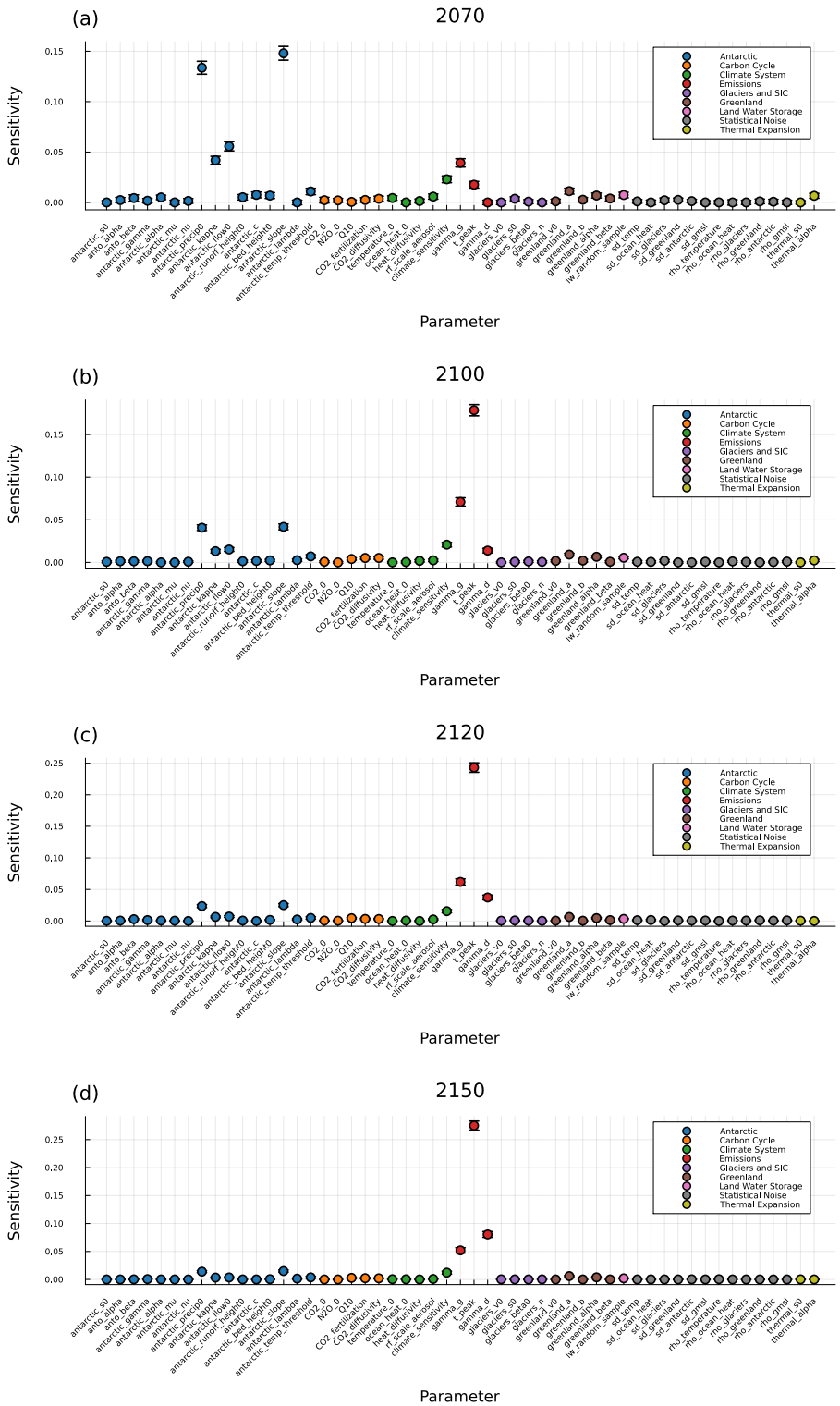

Figure C-6. First-order sensitivity indices for middle peaking samples on decadal timescales.

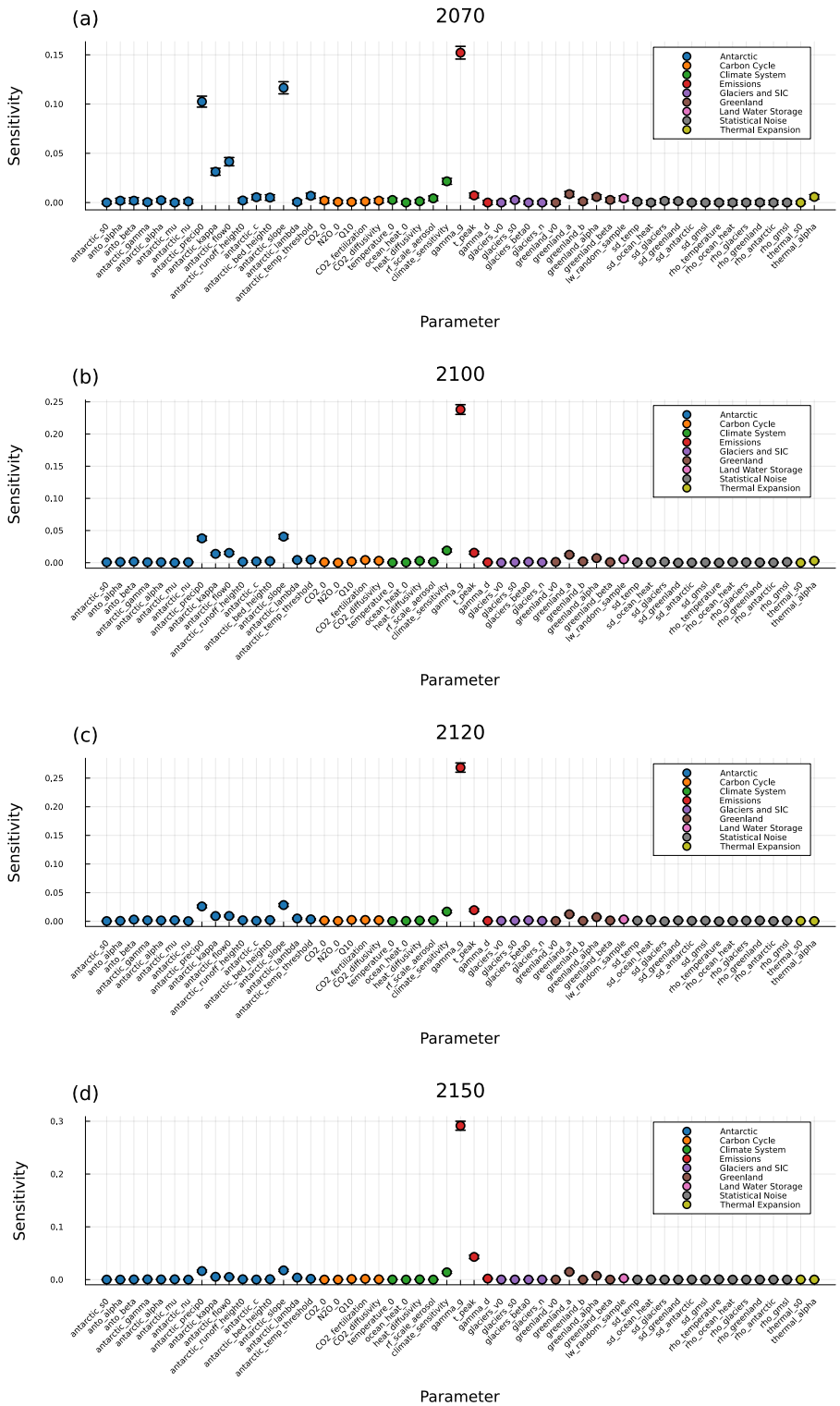

Figure C-7. First-order sensitivity indices for late peaking samples on decadal timescales.